POLITECNICO DI MILANO

Dipartimento di Fisica

ELECTRON SPIN PROPERTIES IN SEMICONDUCTOR HETEROSTRUCTURES

Federico Bottegoni

Ph.D. Dissertation in Physics

Dottorato di Ricerca in Fisica XXIV ciclo

Relator: Prof. Franco Ciccacci
Co-relator: Prof. Henri-Jean Drouhin
Supervisor: Prof. Franco Ciccacci

2009-2011

A Carlo

CONTENTS

Ackowledgments 1

Introduction 2

Part I Spin Polarized Electrons in Ge-Based Heterostructures 4

Introduction 5

1. Electron Spin Polarization and Symmetry 7

1.1 Bulk Germanium 7

1.2 Compressively Strained Germanium 15

2. Spin Polarized Photoemission 19

2.1 Sample growth 19

2.2 High-Resolution X-ray Diffraction 20

2.3 Fundamentals of SPP technique 22

2.4 Experimental results and discussion 24

2.4.1 High-Resolution X-ray Diffraction 24

2.4.2 Quantum Yield 25

2.4.3 Electron Spin Polarization 27

2.4.4 Valence orbital mixing 31

3. Spin Polarized Photo-Luminescence 38

3.1 Fundamentals of SPPL technique 38

3.2 Experimental results 39

Part II Probability-Current and Spin-Current in presence of Spin-Orbit Interaction 48

3.3 Introduction 49

4. General definition of current operators 53

5. Probability current of an effective Hamiltonian 60
5.1 Formulation of the general n^{th}-order Hamiltonian 60
5.2 Velocity operator in presence of SOI interaction 61
5.3 Velocity operator with an effective Hamiltonian $\widehat{H}_{eff}$ 62
5.4 BenDaniel-Duke-like formulation and boundary conditions 66
5.5 The [110]-oriented GaAs barrier 71
5.6 Spin Current 75

ABSTRACT

In the first part of the thesis, the electron spin properties of Ge-based semiconductor heterostructures are studied by means of Spin Polarized Photoemission and Spin Polarized Photo-Luminescence techniques. The in-plane compressive strain and confinement effect, which act on pure Ge grown on $Si_{1-x}Ge_x$ alloy, drastically modifies the band structure so that a very high electron spin polarization can be found in the conduction band of Ge layer, when electrons are excited with circularly-polarized light. This allows the direct detection of optically spin-oriented electron population in the conduction band, which results higher than the bulk one. Furthermore it also possible to obtain an experimental determination of the orbital mixing between Light Hole (LH) and Split Off (SO) bands, away from the Γ point by symmetry analysis based on spin polarization spectra.

In the second part of this thesis, theoretical arguments related to spin transport and dynamics are studied. The common transport operator cannot be properly used, when dealing with Hamiltonian where Spin-Orbit Interaction terms are involved so that a novel definition of probability-current and spin-current operators is given, which satisfies the continuity equation for a general effective Hamiltonian up to the nth order. A reformulation of the boundary conditions at the semiconductor heterostructure interfaces allows the correct determination of the envelope function for tunneling problems and these new findings are applied to the paradigmatic case of an interface, composed of a free-electron-like material and [110]-oriented GaAs barrier.

ACKNOWLEDGMENTS

I would like to thank my PhD supervisor Prof. Franco Ciccacci and Dr. Giovanni Isella for the support, the help and the advices they have been giving me during these three years of experimental activity.

I would like also to thank Prof. Henri-Jean Drouhin, Prof. Guy Fishman and Prof. Jean-Eric Wegrowe because they introduced me in the huge, complicated and difficult world of theoretical physics.

Thanks to Alberto Ferrari for the long hours of experimental and theoretical work spent together.

Thanks also to Prof. Duò and Prof. Finazzi for the interest they have always shown for my activity as all the other components of my research group have done.

Thanks to my father, my mother and my brother Carlo.

Thanks to Barbara.

Thanks to all the people who believed in me.

INTRODUCTION

One of the most exciting field of nowadays condensed matter physics concerns the study of spin-related phenomena: the importance of this topic is basically linked to the possibility of handling the particle spin degrees of freedom that can be eventually employed for a new generation of electronic devices. In this sense, a new branch of solid state physics, known as spintronics, is devoted to the analysis of this subject with particular attention to systems where spin-related effects drastically modify energy and transport properties. Among the huge number of systems that can be considered matter of spintronics study, semiconductors and their heterostructures play a key role, basically because they provide a clear illustration of quantum mechanics and the different interactions can be interpreted closely to atomic physics.

If we wanted to give a definition of this multidisciplinary branch of physics, we could say that *spintronics involves the study of active control and manipulation of spin degrees of freedom in solid state physics* [1]: as a consequence, we can provide two fundamental conceptual steps in the understanding of spin-related phenomena. The first one is the generation of spin polarized carriers and their interaction through the spin relaxation mechanisms and the second one is the study of spin dynamics and transport, which generally differ from the conservation laws of particle transport due to its non-conservative nature [1].

During my PhD activity I had the opportunity to tackle this broad matter both from experimental and theoretical points of view. In the first two years, I have studied the generation and recombination of spin polarized carriers in Ge-based heterostructures with different experimental techniques. At Physics Department of Politecnico di Milano under the supervision of my PhD tutor Prof. Franco Ciccacci, I have set up a dedicated UHV-system for Spin Polarized Photoemission, which has been employed to measure the electron spin polarization in bulk Ge

samples with different doping levels, strained Ge samples and Ge/SiGe Multiple Quantum Wells (MQWs). At the same time, I have developed an experimental set-up for Spin Polarized Photo-Luminescence. This has allowed the study of Ge based- heterostructures, in particular MQWs samples, from a complementary point of view with respect to the photoemission technique. The third year of PhD has been characterized by a six month experience in the research group of Prof. Henri-Jean Drouhin, at Laboratoire des Solides Irradiés in Palaiseau (FR), where I worked on a novel definition of probability and spin current in semiconductors in presence of Spin-Orbit Interaction.

As a consequence of the different activities that I followed, this work is basically divided in two main parts: the first one is devoted to all the results obtained by Spin Polarized Photoemission and Spin Polarized Photo-Luminescence experiments and their interpretation, while the second part is focussed on the theoretical work, concerning particle and spin transport, especially in III-V semiconductor compounds.

Part I

SPIN POLARIZED ELECTRONS IN GE-BASED HETEROSTRUCTURES

Introduction

It is well known that near gap optical pumping with circularly polarized light in III-V semiconductors produces conduction electrons with a degree of electron spin polarization P= $\left(n_{\uparrow}-n_{\downarrow}\right)/\left(n_{\uparrow}+n_{\downarrow}\right)$ where $n_{\uparrow}$ and $n_{\downarrow}$ are the number of excited electrons with spin parallel (s=+1/2) or antiparallel (s=−1/2) to the light wavevector [2]. Selection rules for σ^{+} (σ^{-}) circularly polarized light excitation impose a $\Delta m_j = +1$ $\left(\Delta m_j = -1\right)$ variation of the total angular momentum projection m_j. Since in bulk materials optical transitions to the conduction band minimum at Γ $\left(m_j = m_s = \pm 1/2\right)$ can be excited from the degenerate Heavy Hole (HH) and Light Hole (LH) states ($m_j = \pm 3/2$ and $m_j = \pm 1/2$ respectively) with a relative intensity of 3:1, an upper limit of P= 50% can be obtained. Electrons excited to the Conduction Band (CB) can be extracted into vacuum by lowering the semiconductor vacuum level by means of cesium and oxygen deposition, a procedure known as photocathode activation, thus achieving the so called Negative Electron Affinity (NEA) conditions [3]. The combination of the two phenomena, excitation with circularly polarized light and photocathode activation, gives rise to intense spin polarized photoemission from such materials [4], which is currently being used to produce high efficiency spin polarized electron sources [5]. In order to considerably improve the performance of such sources, materials with higher spin polarization of CB electrons are needed. From the above analysis it appears that a splitting of the degenerate HH and LH bands, as achievable in samples with reduced symmetry such as strained and/or nanostructured semiconductors, including quantum wells, superlattices, and heterojunctions, should give polarization values close to 100%. Pioneering studies of electron spin polarization in nanostructured systems based on III-V semiconductors date back to the eighties [6–10] and more recently the goal of almost completely polarized sources has been essentially achieved, using thin strained layers [11, 12] and strained superlattices [13]. Such sources are currently widely used in electron spectroscopy from solids [14] and in high energy physics as well [15]. Optical orientation attracted a renewed interest in the fields of semiconductor-based spintronics and quantum computation [1], also taking advantage of quantum confinement effects in III-V semiconductor

heterostructures and quantum wells (QWs) [16–18]. In this context it seems very appealing to implement spin functionalities, *i.e.* the control of the spin degree of freedom, in group IV semiconductors, which can be integrated on the well established Si-based electronics platform. However, apart from early investigations [19–21], spin properties in group IV semiconductors have attracted considerable attention only quite recently, when theoretical [22–24] and experimental [25, 26] studies have been carried out. In bulk Ge the energy difference between direct ($E_d = 0.80$ eV) and indirect ($E_i = 0.66$ eV) transitions is only 140 meV at room temperature (RT) and selection rules for circularly polarized light for direct transitions at the Γ point are identical to those applied in the GaAs case. Therefore optical excitation and detection of electron spin polarization is achievable also at the direct band gap of Ge. Due to technological issues related to the 4% misfit between the lattice parameter of Si and Ge, until very recently it has not been possible to exploit such a similarity between the bandstructures of Ge and GaAs. It was only in 2005 that the quantum confined Stark effect, demonstrated more than 20 years ago in GaAs/AlGaAs QWs, has been observed also in Ge/SiGe QWs, nicely evidencing the likeness between the two material systems [27]. Further confirmations of the "quasi direct" nature of Ge QWs are reported in a series of articles recently published by some of us surveying the band alignment type [28], optical absorption selection rules, photo- and electro-luminescence [29] in Ge/SiGe QWs. These last studies rely on the availability of epitaxial samples with high structural quality, grown in our laboratories by Low Energy Plasma Enhanced Chemical Vapour Deposition (LEPECVD) [30]. In this chapter we report on spin polarized photoemission from such high quality Ge based heterostructures, namely thin strained Ge films grown on relaxed $Si_{1-x}Ge_x$ substrates and multiple quantum well (MQW) systems formed by Ge wells surrounded by $Si_{1-x}Ge_x$ barriers. The layout of this chapter is the following: Sec. 1 is devoted to the analysis of the electron spin polarization through the group theory, either in bulk structures, either in strained and confined IV group heterostructures. In Sec. 2 the Spin Polarized Photoemission technique is presented and all the experimental measurements on IV group semiconductor heterostructures are analyzed, while Sec. 3 is focussed on the experimental set-up and results of Spin Polarized Photo-Luminescence measurements.

1. ELECTRON SPIN POLARIZATION AND SYMMETRY

1.1 Bulk Germanium

The possibility to optically generate in the conduction band of a solid a population of spin polarized electrons, where the electron spin polarization is defined as P= $(\langle S_x \rangle, \langle S_y \rangle, \langle S_z \rangle)$, can be basically exploited in a wide number of systems. This is the consequence of the fact that the only two experimental requirements are the excitation of the electrons with circularly-polarized light of convenient energy and the choice of at least one state of a band, involved in the transition, where Spin-Orbit Interaction (SOI) has removed the orbital degeneration [2, p. 297].

In this context it is relevant the notion of group of the wave-vector $G_{\mathbf{k}}$, by which it is possible to classify the Bloch states (for the moment the spin-dependent part of the wave-function is not taken into account) with respect to the symmetry operations that make the wave-vector **k** invariant. Indeed $G_{\mathbf{k}}$ is always a subgroup of a symmorphic space group G so that when applied to symmetry points or lines of the Brillouin zone, it can be considered as one of the 32 point groups. Then all the Bloch functions with a general wave-vector **k** can be associated to a set of symmetry transformations, according to an irreducible representation of $G_{\mathbf{k}}$, which can be conveniently called Γ^{α}. Considering the particular column of this matrix representation, all the properties of the different wave-functions can be known. When SOI is introduced, the Bloch states have to be written as spin-dependent wave-functions. Then, beside the irreducible representation Γ^{α} of $G_{\mathbf{k}}$, also the irreducible representation $D_{\frac{1}{2}}$ of the Full Rotation Group has to be added, consisting in the spin-basis functions $|\uparrow\rangle$ and $|\downarrow\rangle$. In this case, the final representation of the spin dependent Bloch states is given by the direct product $\Gamma^{\alpha} \times D_{\frac{1}{2}}$. This direct product is generally reducible and it is the sum of

one or more representations, irreducible with respect to the correspondent double group. This means that a generic Bloch state will be written as linear combination of functions belonging to different double group representations, of which the coefficients are called Coupling Coefficients (CC). This procedure enlights the fact that the introduction of SOI terms can remove the orbital degeneracy because it can provide a symmetry reduction of the system.

Once evaluated the symmetry of the Bloch states, the further fundamental point to be taken into account is the symmetry of the dipole operator in the matrix elements, which describes the transition of an electron from an initial to a final state under excitation with circularly-polarized light. Indeed in dipole approximation the expression of the electromagnetic perturbation $\mathrm{O}(\mathbf{r},t)$, limited to vertical transitions only, is $\mathrm{O}(\mathbf{r},t) \approx \mathbf{a_0} \cdot \mathbf{p}$ [31]. By taking the z-axis along the **k**-direction of the electrons involved in the transition, it is straightforward to obtain the explicit expression of the operator which represents the incident circularly-polarized light with $\mathrm{O}(\mathbf{r},t) \approx p_x - (+)ip_y$, where the sign - (+) applies to right (left) polarization of the incident light. At this point, we introduce the convenient representation of the momentum operator Γ^p and the matrix element of the considered transition can be evaluated through the well-known Wigner-Eckhart Theorem [32], in the generalized form proposed by Koster, which properly applies to point and space symmetry groups [33]. Following the conceptual scheme above, it is easy to show, for example, that the polarization at the Γ point for all the III-V zincoblende semiconductors is the same [2, p. 298].

Evidently, a higher electron spin polarization can be found at high symmetry points of the Brillouin zone, because there the influence of SOI is strongest while generally the polarization is zero when considered on a general point of the Brillouin zone without particular symmetry properties.

Due to the fact that all the experimental measurements, presented in this part, are related to Ge-based heterostructures, in the following we will focus on the application of group theory to systems with diamond-like structure, which have the Brillouin zone of Fig. 1.1. Among them, clearly bulk Ge plays a key role: in particular the Γ point and the Δ line of the Brillouin zone of bulk Ge will be taken into account. Indeed we consider the Γ point of coordinates (0,0,0) of the face centered cubic lattice (fcc) and we take into account the O_h^7 space

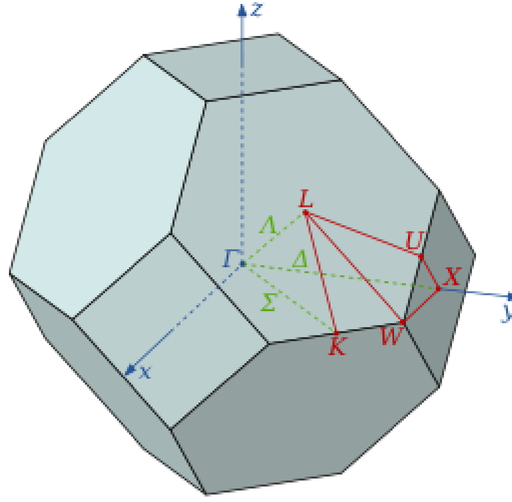

Fig. 1.1: Brillouin zone for fcc lattices, where all the relevant symmetry (blue and red) points and (green) lines are considered.

group. Care has to be taken because O_h^7 is not symmorphic: in fact there are 24 elements, associated to the inversion, that are not at (0,0,0) but at $(\frac{1}{8}a, \frac{1}{8}a, \frac{1}{8}a,)$, a being the lattice constant. However, except for particular symmetry points as *X, W, Z* [34], the common tables for the corresponding symmorphic space groups can be employed [2, p. 334]. In the following all the different representations Γ^{α} will be written according to the Bouckaert, Smoluchowski and Wigner (BSW) notation: if the reader is more familiar with the Koster (K) notation, a useful table of conversion between the two notations is provided by Yu and Cardona [35, p. 40, Table 2.7]. Then we consider the O_h point group which corresponds to the wave-vector group $G_{(0,0,0)}$: for sake of clarity, we refer to the bulk Ge band structure scheme of Fig. 1.2, as calculated by Yu and Cardona [35]. At the bottom of the conduction band the orbital part of the wave-function has $\Gamma^{2'}$-symmetry. This is a one-dimensional representation for the O_h group, which must be properly changed in the presence of SOI: the inspection of the Character Table for the O_h group suggests that $D_{\frac{1}{2}}$ transforms as Γ_6^+ [36, p.103, Table 87]. Consequently the functions belonging to this representation provide a good basis to write the spin dependent part of the wave-function and the direct product $\Gamma^{2'} \times \Gamma_6^+ = \Gamma_7^-$ directly gives the double group representation of the corresponding Bloch state. At the top of the valence band the situation is a little more involved: in absence of SOI,

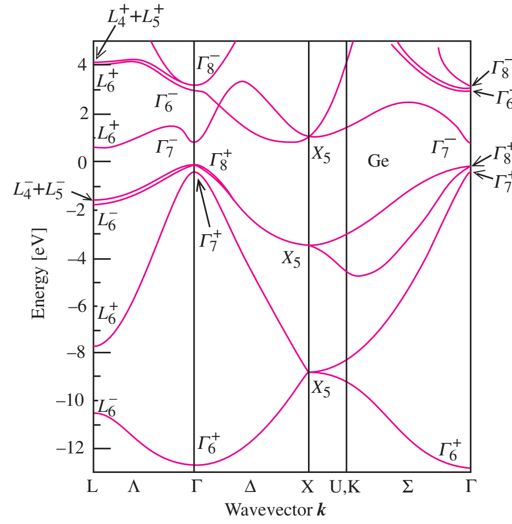

Fig. 1.2: Band structure of bulk Ge [35].

we have 6-fold degenerate states with $\Gamma^{25'}$-symmetry. Again, being Γ_6^+ the good representation for the spin wave-functions, we have to evaluate the direct product $\Gamma^{25'} \times \Gamma_6^+ = \Gamma_8^+ + \Gamma_7^+$. We can see that in this case the presence of SOI partially removes the degeneration at the top of the valence band, lowering the symmetry of the system and providing the so called Heavy Hole (HH) and Light Hole (LH) band of Γ_8^+-symmetry, lifted from the Split-Off (SO) band of Γ_7^+-symmetry [37].

Now, in order to evaluate the electron spin polarization obtained through transitions across the direct energy gap, we have to express these states as linear combination of functions belonging to the proper representations, of which the coefficients are the CC ones. However, following the procedure of Ref. 20, under spherical approximation we can still use the unique irreducible representation of the Full Rotation Group, of which the basis functions are the spherical harmonics Y_l^m. Thus the wave-functions are written in terms of Y_l^m and spin functions $|\uparrow\rangle$, $|\downarrow\rangle$, where the correct symmetry is provided by the Clebsh-Gordon coefficients [38, p. 123, Table 5-2]. Under the same approximations, the operator $O(\mathbf{r},t)$ can be represented through the spherical harmonics Y_1^{-1} and Y_1^1, depending on the left or right circular polarization of the exciting light. The transition scheme is shown in Fig. 1.3. If we take the z-axis of the system along the direction of the incident light and we suppose to resonantly excite electrons across the Ge direct gap, we

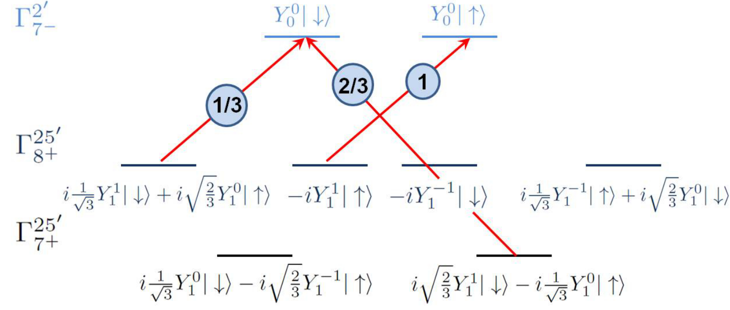

Fig. 1.3: Scheme of the direct transitions at the Γ point of bulk Ge. According to the spherical approximation, the wave-functions can be expressed in terms of linear combination of products between spherical harmonics and spin functions, while the relative intensity of every transition is given in circles. The symmetry of the different states is written on the left of the scheme, with a notation where the superscript denotes the single group representation, while the subscript the double group one. Only transitions with left-circularly polarized light are shown, i.e. where $\mathrm{O}(\mathbf{r},t)$ has Y_1^{-1} symmetry.

can calculate the electron spin polarization at the bottom of the conduction band as P$= (0,0,\langle S_z\rangle) = \left(n_\uparrow - n_\downarrow\right) / \left(n_\uparrow + n_\downarrow\right)$, where $n_{\uparrow(\downarrow)}$ is the number of electrons with up (down) spin. Thus theoretical and experimental results prove that P$= 50\%$ [20].

In order to better explain the crucial concept of this section, *i.e.* the fact that P depends only on the symmetry of the states involved in the transitions, we now consider direct transitions that are not exactly at the Γ point of the Brillouin zone, but along the Δ line. The reason to analyze this interesting situation is that an experimental limit in photoemission experiments does not allow to detect P at the Γ point [39]: neverthless, Allenspach *et al.* have shown that a polarization equal to 50% can be measured at T$= 40$ K in the proximity of the Γ point, but involving Bloch states along the Δ line of bulk Ge [20]. The situation is shown in Fig. 1.4: taking into account the C_{4v} point group, the final state has $\Delta_7^{2'}$-symmetry, whereas the valence initial states have respectively Δ_6^5, Δ_7^5 and $\Delta_7^{2'}$-symmetry. Considering transitions in the proximity of the Γ point, which retain the symmetry labels of the Δ direction, we can argue that the two direct transitions $\Delta_6^5 \rightarrow \Delta_7^{2'}$ and $\Delta_7^5 \rightarrow \Delta_7^{2'}$ are not sufficient to explain a net spin polarization, being their intensity I_u and I_d equal. This is why it is necessary to introduce the hybridization between Bloch states along the Δ line. At the Γ point all the wave-functions of the topmost valence band have the same orbital symmetry, *i.e.* $\Gamma^{25'}$, so that

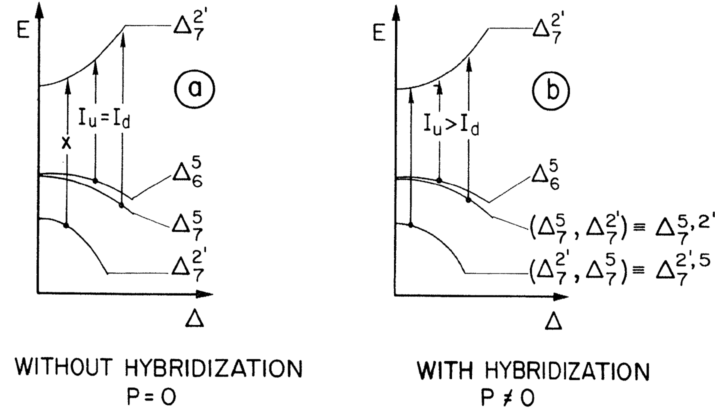

Fig. 1.4: Symmetry and scheme of the direct transitions along Δ line of bulk Ge (C_{4v} point group). a) symmetry of initial and final states without taking into account the hybridization of Δ_7^5 state: in this case the two transitions $\Delta_6^5 \to \Delta_7^{2'}$ and $\Delta_7^5 \to \Delta_7^{2'}$ have the same intensity I_u and I_d so that the polarization P is zero. b) symmetry of initial and final states with hybridization of Δ_7^5: the two transitions $\Delta_6^5 \to \Delta_7^{2'}$ and $\Delta_7^{5,2'} \to \Delta_7^{2'}$ do not have the same intensity, because the forbidden transition $\Delta_7^{2'} \to \Delta_7^{2'}$ removes intensity from I_d, then P results equal to 50% [20].

all the symmetrized functions are automatically combined through the Coupling Coefficients by the same point group table, in this case O_h in order to give HH, LH and SO states. Consequently SOI removes the degeneration between such states. Along the Δ line, due to the different orbital symmetry of the involved states, we have to combine symmetrized functions that belong to different single group representations in order to generate a wave-function with a mixed character. The coefficients of this linear combination cannot be the Coupling Coefficients; thus they must be determined experimentally. With this procedure, it is possible to build up wave-functions of mixed symmetry for $\Delta_7^{5,2'}$ states, as shown in Fig. 1.4. At this purpose we consider the C_{4v} point group and the symmetrized product functions $u_i^{\alpha} v_{m_s}^{\beta}$. Here u_i^{α} is the orbital function, belonging to the α-representation with $i = x, y$, while $v_{m_s}^{\beta}$ is the spin function, belonging to the β-representation with $m_s = \pm 1/2$. Inspection of the Full Rotation Group compatibility table for C_{4v} shows again that the spin-dependent part of the wave-functions transform as Γ^6 [36, p. 48, Table 38], then final states of $\Delta_7^{2'}$ (Γ^4) symmetry can be written as [36, p. 46, table 35]:

$$\psi^7_{\frac{1}{2}} = -iu^4 v^6_{\frac{1}{2}};$$
$$\psi^7_{-\frac{1}{2}} = iu^4 v^6_{-\frac{1}{2}}. \quad (1.1)$$

For sake of clarity, it is useful to remark that the unidimensional representation Γ^4 of Eq. 1.1 is obtained considering the Compatibility Table for O_h [36, p. 104, Table 88]. Let us also note that the initial representation $\Gamma^{2'}$ transforms as Γ^4 when applied to the C_{4v} group. Since their orbital symmetry does not allow any hybridization with the other states, initial states of Δ^5_6 (Γ^5) symmetry can be simply expressed as [2, p.339]:

$$\psi^6_{\frac{1}{2}} = \frac{i}{\sqrt{2}} u^5_x v^6_{\frac{1}{2}} + \frac{1}{\sqrt{2}} u^5_y v^6_{\frac{1}{2}},$$
$$\psi^6_{-\frac{1}{2}} = -\frac{i}{\sqrt{2}} u^5_x v^6_{-\frac{1}{2}} + \frac{1}{\sqrt{2}} u^5_y v^6_{-\frac{1}{2}}, \quad (1.2)$$

where $u^5_{x,y}$ correspond to the p-like orbital wave-functions. On the contrary, $\Delta^{5,2'}_7$ symmetry states are written as linear combination of symmetrized functions of Δ^5_7 (Γ^5) and $\Delta^{2'}_7$ (Γ^4) symmetry in order to take into account the hybridization with the SO band of Fig. 1.4, with coefficients which are directly derived from the fact that the measured P is equal to 50% and this value must approach with continuity the P value at the Γ point. Introducing also the condition of normalization between the two coefficients we get [2, p.339]:

$$\psi^7_{\frac{1}{2}} = \frac{1}{\sqrt{3}} \cdot \psi^5_{-\frac{1}{2}} + \sqrt{\frac{2}{3}} \cdot \psi^{2'}_{\frac{1}{2}} = \frac{1}{\sqrt{3}} \left[-\frac{i}{\sqrt{2}} u^5_x v^6_{-\frac{1}{2}} - \frac{1}{\sqrt{2}} u^5_y v^6_{-\frac{1}{2}} \right] + \sqrt{\frac{2}{3}} \left[u^4 v^6_{\frac{1}{2}} \right],$$
$$\psi^7_{-\frac{1}{2}} = \frac{1}{\sqrt{3}} \cdot \psi^5_{\frac{1}{2}} - \sqrt{\frac{2}{3}} \cdot \psi^{2'}_{-\frac{1}{2}} = \frac{1}{\sqrt{3}} \left[\frac{i}{\sqrt{2}} u^5_x v^6_{\frac{1}{2}} - \frac{1}{\sqrt{2}} u^5_y v^6_{\frac{1}{2}} \right] - \sqrt{\frac{2}{3}} \left[u^4 v^6_{-\frac{1}{2}} \right]. \quad (1.3)$$

The explicit expression of the states with $\Delta^{2',5}_7$ symmetry is not shown, because at this point we are interested in optical processes involving only the lowest

conduction states and HH-LH (nearly degenerate) valence states. Regarding this appealing case, where the experimental results are applied to obtain the hybridization coefficients, we develop the calculations to show that under the assumptions above, the experimental P value can be obtained. At this purpose, we consider the operator $O(\mathbf{r},t)$ that represents the incident left-circularly polarized light along the z-direction, again considered parallel to the wave-vector of excited electrons. We can write:

$$O(\mathbf{r},t) \approx p_x - ip_y, \tag{1.4}$$

which belongs to Δ^5 (Γ^5) representation, transforming as (S_x, S_y) [36, p. 45, Table 33]. At this point we show the expressions of the two only transitions which are possible with the left-polarized incident light of Eq. 1.4:

$$\begin{aligned} I_u &= |\langle -iu^4 v^6_{\frac{1}{2}} | p^5_x - ip^5_y | \frac{i}{\sqrt{2}} u^5_x v^6_{\frac{1}{2}} + \frac{1}{\sqrt{2}} u^5_y v^6_{\frac{1}{2}} \rangle|^2, \\ I_d &= |\langle iu^4 v^6_{-\frac{1}{2}} | p^5_x - ip^5_y | \frac{1}{\sqrt{3}} \left[-\frac{i}{\sqrt{2}} u^5_x v^6_{-\frac{1}{2}} - \frac{1}{\sqrt{2}} u^5_y v^6_{-\frac{1}{2}} \right] + \sqrt{\frac{2}{3}} \left[u^4 v^6_{\frac{1}{2}} \right] \rangle|^2. \end{aligned} \tag{1.5}$$

Without performing any calculation, it is possible to see that the matrix elements between states with opposite spin dependent wave-functions vanish due to the fact that $\langle v^6_{-\frac{1}{2}} | v^6_{\frac{1}{2}} \rangle = 0$: then looking at the expression of I_d, the component of the matrix element that concerns the transition $\Delta^{2'}_7 \rightarrow \Delta^{2'}_7$ removes intensity from I_d. Finally, we derive the intensity of the transitions above:

$$\begin{aligned} I_u &= |ic^5_{4,5}|^2, \\ I_d &= \frac{1}{3} \cdot |c^5_{4,5}|^2, \end{aligned} \tag{1.6}$$

where $c^5_{4,5}$ is the unknown factor which comes from the product of the different functions involved in the matrix elements of Eqs. 1.5. Then we can calculate the electron spin polarization P along the z-direction:

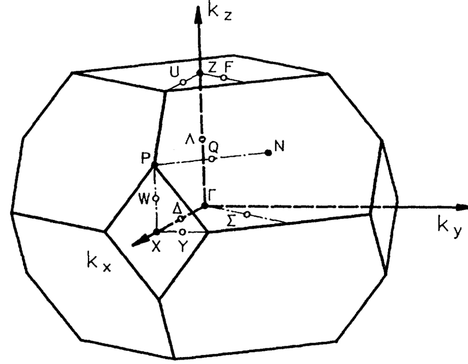

Fig. 1.5: Brillouin zone of pure Ge grown on (001) Si substrate [41]. k_z is the growth direction.

$$P = (0,0,\langle S_z \rangle) = \frac{-|c^5_{4,5}|^2 + \frac{1}{3}\cdot|c^5_{4,5}|^2}{-|c^5_{4,5}|^2 - \frac{1}{3}\cdot|c^5_{4,5}|^2} = 50\%. \tag{1.7}$$

1.2 Compressively Strained Germanium

The symmetry arguments that have been exploited in Sec. 1.1 to obtain coherent expressions of the Bloch wave-functions in bulk Ge, can be evidently applied when considering strained Ge layers. In the following we will refer only to the paradigmatic heterostructure, composed of pure Ge grown on (001) Si, basically for two reasons. First, all the samples of Sec. 2 have such a growth direction, second the theoretical treatment of this heterostructure is quite simple with respect to more complicated higher quality heterostructures, which present a virtual substrate (buffer layer) of $Si_{1-x}Ge_x$ alloy [30, 40]. The lattice mismatch between Ge and Si is 4%, so that a layer of pure Ge grown on a (001) substrate of pure Si undergoes a biaxial compressive strain in the growth plane.

The present discussion will be focussed on the Γ point, on the Δ line and on the Λ line (growth direction) of the distorted Brillouin zone of Fig. 1.5, according to the experimental data that shall be presented in Sec. 2. The space group that has to be taken into account in this case is D^{19}_{4h}: then at the Γ point the group of the wave-vector $G_{(0,0,0)}$ is identified as the D_{4h} point group. The inspection of the compatibility table between O_h and D_{4h} [36, p. 104, Table 88] shows

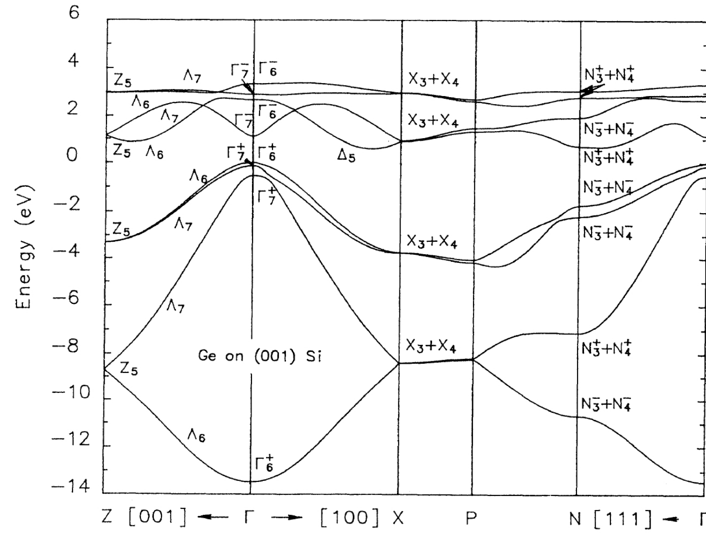

Fig. 1.6: Band structure of compressively strained Ge grown on (001) Si substrate, where all the symmetry points and lines of the tetragonally distorted Brillouin zone are represented [41]. [001] is the growth direction while [100] represent the two equivalent in-plane directions.

that the bottom of the conduction band of Γ_7^--symmetry, is unaffected by the presence of the compressive strain, while the Γ_8^+ representation, related to the HH-LH bands, is reducible and decomposes in the two irreducible representations Γ_6^+ and Γ_7^+. This basically means that the degeneration between HH and LH bands, present in bulk Ge, is completely lifted due to the distortion of the Brillouin zone. Finally, being the SO band of Γ_7^+ symmetry, its representation is unchanged after the introduction of a strain component. Evidently group theory cannot estimate the energy difference which arises between states of Γ_6^+ and Γ_7^+-symmetry: nevertheless, calculations based on the deformation potential theory [42] and tight-binding approach [41] provide values of the HH-LH splitting of the order of tens meV and a higher energy difference between LH and SO states is also expected [43–48].

Indeed, the importance of this kind of heterostructure is given by the fact that a process of optical orientation like the ones discussed in Sec. 1.1, can lead to a 100% spin polarized electron population at the bottom of the conduction band, provided that the energy of the incident light is chosen resonant (or quasi-resonant) to the direct energy gap. In fact, under spherical approximation, the

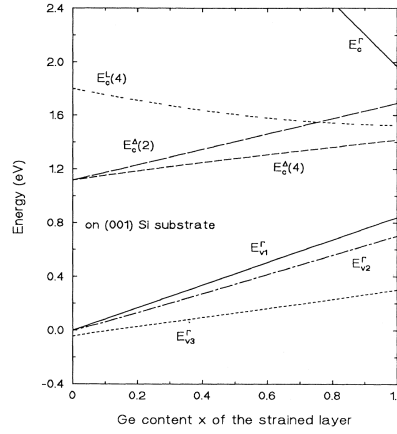

Fig. 1.7: Valence and conduction band-edge variation with Ge content of the $Si_{1-x}Ge_x$ alloy, grown on a (001) Si substrate [41].

conceptual scheme of Fig. 1.3 can be exploited also in this case: it is not an abrupt aproximation, due to the fact that the perturbation induced by the strain term provides an energy difference between HH and LH states which is small with respect to the direct energy band of the system. Then the spherical harmonics are still good basis functions to represent Bloch states at the Γ point. The only difference with respect to the transition scheme of Fig. 1.3 is the removal of the degeneration between HH and LH states, which allows the excitation of a fully spin polarized electron population from HH state only. We now move to analyze the crystallographic direction [100], or the Δ line: as a consequence of the in-plane biaxial strain, the symmetry group is reduced so that all the representations $\Delta_7^{2'}$, Δ_6^5 and Δ_7^5 reduce to the Δ_5 representation [36, p. 47, Table 36], then providing the same basis functions for all the Bloch states. Finally, we analyze the effect of the compressive biaxial strain along the growth direction, which is an interesting direction for direct transitions and photoemission experiments, when the wave-vector **k** of the excited electrons is considered parallel to this direction. The symmetry of the crystal is not reduced by the strain and all the symmetry labels, which describe the irreducible representations along the [001] direction of bulk Ge still hold. In the present case, along the crystallographic direction $\Gamma \to Z$, conduction states have Λ_7 symmetry, while HH and LH states have respectively Λ_6 and Λ_7-symmetry, where only the irreducible double group representations are

shown, being the single group ones always the same. In order to complete the discussion, Fig. 1.7 shows the valence and conduction band-edge variations when a heterostructure $Si_{1-x}Ge_x$ grown on Si(001) is considered: for the extreme case that we are discussing, namely pure Ge grown on Si(001), we can see that both the direct and indirect energy gap increase linearly with the strain degree, *i.e.* the percentage of Ge in the $Si_{1-x}Ge_x$ alloy. If we assume that a thin layer of pure Ge is grown on a virtual substrate composed of a $Si_{1-x}Ge_x$ alloy with a given Ge percentage and we neglect the plastic relaxation of the layer, Fig. 1.7 can help us to evaluate the band structure at the Γ point of such an heterostructure.

2. SPIN POLARIZED PHOTOEMISSION

This section is devoted to the activity developed at Physics Department of Politecnico di Milano: in the following we shall briefly discuss the growth of the Ge-based heterostructure samples that have been employed for Quantum Yield (QY) and Spin Polarized Photoemission (SPP), the fundamentals of SPP technique, the experimental set up and the measurement results that have been obtained.

2.1 Sample growth

LEPECVD is a versatile growth technique which has been used to obtain high quality group IV heterostructures [30]. In order to study the main Ge-based nanostructures, suitable for spintronics applications, three fundamental sample structures have been employed: Ge-on-Si epilayers, strained Ge epilayers, and Ge/SiGe MQWs. The gradual reduction of the symmetry of the systems involved provides insight into the properties of group IV heterostructures as emitters of polarized electrons. The Ge-on-Si sample (Fig. 2.1a) is a 1 μm thick heavily B-doped Ge layer, directly grown on a Si(001) wafer. This can actually be considered as bulk-like Ge film, in fact the layer thickness is well above the critical thickness for pure Ge directly grown onto Si, resulting in the complete relaxation of the lattice mismatch strain. The bulk-like behavior of this heterostructure was confirmed by comparing its photoemission spectra with that of a p-type Ge wafer. The strained Ge epilayer structure is shown in Fig. 2.1b: a high quality relaxed virtual substrate (VS) is graded from pure Si to $Si_{1-x}Ge_x$, with a grading rate of $0.07/\mu$m; when the desired Ge content in the alloy is achieved, a constant composition $Si_{1-x}Ge_x$ buffer layer is grown. Finally a compressively strained Ge layer is deposited. By varying the VS final Ge content from 0.5 to 0.8,

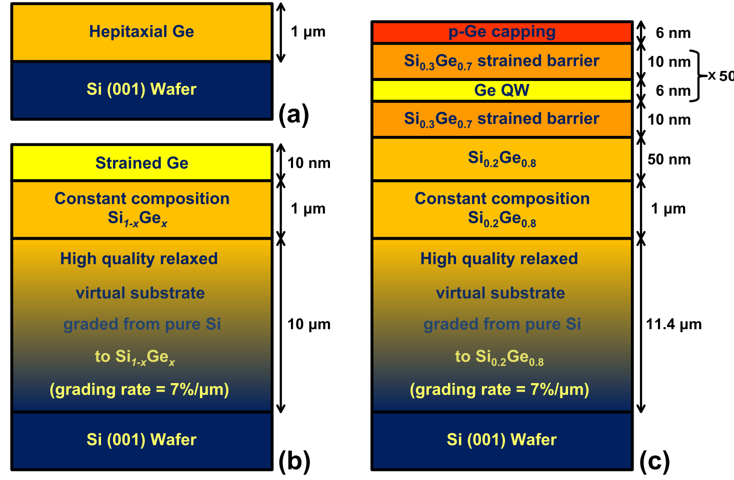

Fig. 2.1: Scheme of the sample structure: (a) Ge-on-Si epilayer; for a thickness of 1 μm the pure Ge layer is fully relaxed and has been used as a bulk-like reference in our work. (b) Strained Ge/SiGe; samples with a final Ge content x in final virtual substrate varying between 0.50 to 0.80 have been investigated. (c) $(Si_{0.3}Ge_{0.7}/Ge)\times 50/Si_{0.2}Ge_{0.8}$ Multiple Quantum Wells.

we induced different levels of biaxial compressive strain $\varepsilon = \left(a_{||} - a_{Ge}\right)/a_{Ge}$ in the Ge layers being $a_{||}$ and a_{Ge} the in-plane lattice parameters of the strained Ge epilayer and of bulk Ge, respectively. The Ge fraction x also determines the critical thickness above which the Ge layer relaxes: the higher the final Ge content x of the relaxed VS, the lower is the lattice mismatch between pure Ge and $Si_{1-x}Ge_x$ and the greater is the critical thickness. The critical thickness for the Ge layers investigated have been calculated using the Matthews force balance model [49] and are reported in Table 2.1. Finally, Fig. 2.1c shows the growth scheme of the $(Si_{0.3}Ge_{0.7}/Ge)\times 50/Si_{0.2}Ge_{0.8}$ MQW sample comprising 50 periods of 5 nm thick Ge wells and 10 nm $Si_{0.3}Ge_{0.7}$ barriers grown on a $x = 0.80$ VS. The structure is terminated by a 6 nm thick Ge layer.

2.2 High-Resolution X-ray Diffraction

HRXRD measurements were performed using a PANalytical X'Pert PRO MRD diffractometer. A hybrid 2-bounce asymmetric Ge(220) monochromator, which includes an x-ray mirror, was used on the primary beam in order to select

sample	schematic structure	critical thickness [nm]	thickness [nm]	nominal $\varepsilon_{\|\|}$ [%]	measured $\varepsilon_{\|\|}$ [%]
56455	Ge/Si	1	1000	0	+0.05
8492	$Ge/Si_{0.5}Ge_{0.5}$	4	10	-2	-0.86
8491	$Ge/Si_{0.38}Ge_{0.62}$	5	10	-1.60	-1.13
8493	$Ge/Si_{0.31}Ge_{0.69}$	8	10	-1.20	-0.96
7949	$Ge/Si_{0.28}Ge_{0.72}$	8	10	-1.20	-0.89
8509	$Ge/Si_{0.2}Ge_{0.8}$	13	10	-0.82	-0.71
8422	$(Si_{0.3}Ge_{0.7}/Ge)\times 50/Si_{0.2}Ge_{0.8}$	-	-	-0.82	-0.74

Tab. 2.1: The structural properties of the collection of analyzed samples is shown for every configuration in terms of critical thickness, nominal Ge layer thickness, and nominal and measured in-plane strain. A maximum strain of -1.13% is reached for the $Ge/Si_{0.4}Ge_{0.6}$ structure #8491; most structures (apart from #8509) show some degree of strain relaxation of the Ge layer. In the case of the thick Ge/Si structure #56455, a small degree of tensile strain is present due to the mismatch of thermal expansion coefficients of Ge and Si.

the intense Kα 1 line from the Cu x-ray tube. The monochromator was fitted with a programmable attenuator, in order to prevent the brightest peaks from saturating the detector. A 3-bounce symmetric analyzer crystal was mounted in front of the detector for high-resolution mapping. Reciprocal space maps (RSM), in the (004) and (224) grazing-incidence geometries, were typically acquired with a 0.5 s step-time and angular steps of 0.01° or 0.02°, with a 5.0 s step-time used to map the Ge peak in more detail. In all cases, the positions of diffraction peaks from epitaxially grown layers was considered with respect to the Si substrate peak, which provides an absolute calibration reference. The (004) geometry probes only the lattice planes parallel to the Si(001) substrate surface. It is therefore sensitive to the out-of-plane lattice parameter and the tilt of these planes (induced by the strain relaxation process in the virtual substrate) with respect to the substrate. Information on the in-plane lattice parameter can be obtained from the (224) reflections. The Ge content and strain ε in the epitaxial layers were then calculated using the lattice parameter data in Ref. 50 and linear interpolation of the lattice constants of Si and Ge given in Ref. 51. Spin polarized photoemission experiments require an high temperature annealing step which might modify the strain state of the Ge epilayers. In order to take this into account, all HRXRD measurements here have been performed after photoemission ones.

2.3 Fundamentals of SPP technique

After growth the samples were inserted in an ultra high vacuum chamber (pressure below 3×10^{-10} torr) where spin polarized photoemission (SPP) was performed: the experimental apparatus is schematically shown in Fig. 2.2a. According to standard methods, the samples were heat-cleaned at 600 °C and then activated by alternate exposure to Cs and O_2 following the so called yo-yo procedure [3, 5, 52]. The activation was routinely monitored by measuring the photocurrent while illuminating the sample with a few mW He-Ne laser. In the final steps the He-Ne laser was replaced by near infrared irradiation (1.4 eV) in order to optimize the photosignal at threshold. The minimum photon energy for which a photocurrent signal clearly emerged from noise was always larger than 1.2 eV, well above the Ge energy gap, indicating a non-NEA condition, as usual in Ge based photocathodes [20, 39]. The photoelectron spin polarization P and quantum yield Y were measured as a function of the photon energy without any energy filtering on the emitted electrons. All measurements reported here were performed at 120 K. Activated samples were illuminated by an optical system producing circularly polarized light (Fig. 2.2a). A quartz halogen lamp was used as a light source; after monochromatization and collimation, circularly polarized light was produced by means of a wide range $\lambda/4$ retarder. The optical system was calibrated in terms of light intensity and circular polarization, the latter being larger than 95% over the full photon energy range investigated. The photon energy resolution is around 5 meV, smaller than the HH-LH energy splitting expected in our samples [28, 53]. Photoemitted electrons were collected by an electron optics system including a 90° rotator [54], which transforms the beam polarization from longitudinal to transverse, as required for Mott polarimetry [55]. The beam is then sent into a medium-energy spherical retarding field Mott detector [55], where it impinges on a Au target with scattering energy in the 10-20 keV range (Fig. 2.2b). The Mott detector efficiency has been calibrated according to standard methods [55], yielding a Sherman function $S = 0.09 \pm 0.01$ at 20 keV, in agreement with reported values in similar conditions [55]. The uncertainties on S give a 10% systematic relative error on the measured polarization values. However this does not influence relative measurements. The overall calibration

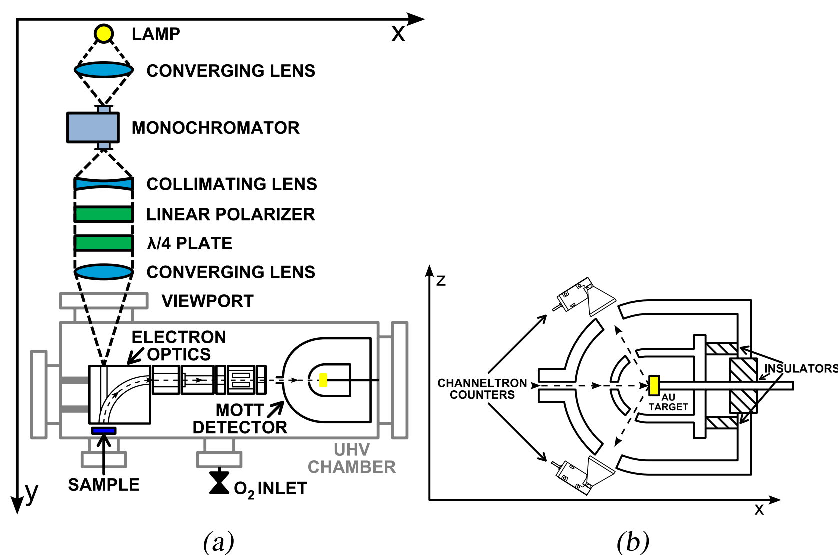

Fig. 2.2: (a) Sketch of the experimental apparatus for spin polarized photoemission measurements. The optical system includes a CM 110 Compact 1/8 Meter Monochromator with a Czerny-Turner design and an Achromatic Quartz and MgF_2 $\lambda/4$ retarder. The photoelectron spin polarization is along the y-axis (the quantization axis is given by the light propagation direction): the initially longitudinally polarized beam is transformed into a transversally polarized one by the 90° rotator before being accelerated into the Mott detector. (b) Schematic diagram of the spherical retarding field Mott polarimeter, note that the plane of this figure is rotated by 90° with respect to that of Fig. 2.2a.

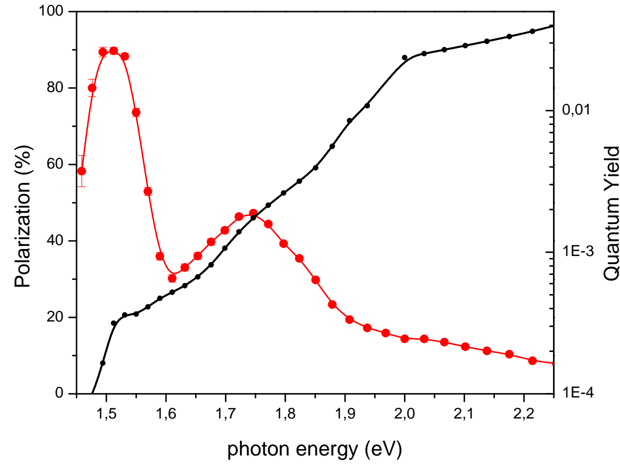

Fig. 2.3: Spin polarization and quantum yield spectra from the St. Petersburg optimized photocathode based on a strained AlInGaAs/AlGaAs superlattice: for near threshold excitation P values around 90% are achieved, *i.e.* the photoelectrons are almost completely polarized. The spectral shape of both polarization and quantum yield are identical to those reported in the original work [13]. Regarding the polarization, even the absolute value is identical.

was independently checked by measuring reference spectra from III-V based photocathodes, including bulk GaAs and an AlInGaAs/AlGaAs superlattice [13]. The P($h\nu$) spectrum from the latter photocathode, shown in Fig. 2.3, is indeed in very good agreement with the reported one [13].

2.4 Experimental results and discussion

2.4.1 High-Resolution X-ray Diffraction

Table 2.1 summarizes the results of HRXRD measurements. As an example, RSMs are shown for sample 8509 in Fig. 2.4. The Si substrate peak is seen at $q_\perp = 4/a_{Si} = 7.37\ nm^{-1}$. In the (004) RSM the main features are centred on the line $q_{||} = 0\ nm^{-1}$, indicating a lack of a net tilt in the epitaxial layers. The graded part of the VS gives rise to the diffuse scattering between the Si peak and the 2μm $Si_{0.2}Ge_{0.8}$ layer peak at $q_\perp = 7.13\ nm^{-1}$. This strong peak is broadened in the $q_{||}$ direction due to mosaicity. The 10 nm strained Ge layer can be seen as a weak peak, broadened in $q_\perp$ by about $\Delta q \approx 1/(10\ nm) = 0.1\ nm^{-1}$, at $q_\perp = 7.04\ nm^{-1}$.

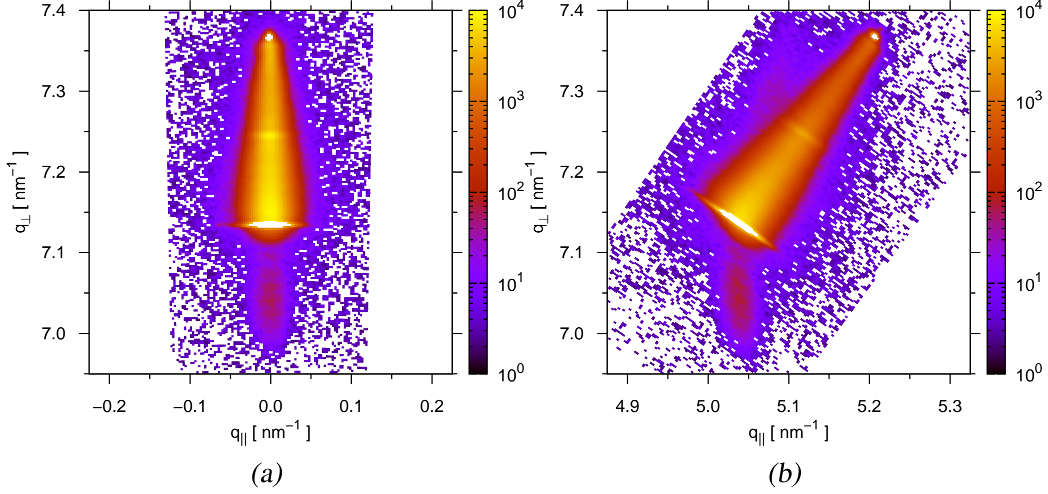

Fig. 2.4: RSMs about the (004) (a) and (224) (b) Bragg peaks of the sample 8509. $q_\perp$ is along the [001] direction and $q_{||}$ is along the [110] direction. The Si substrate peak is at $q_\perp = 7.37$ nm^{-1}. The VS can be seen down to about 7.13 nm^{-1}, and the thin strained Ge layer itself is visible at 7.04 nm^{-1}. The logarithmic intensity scale is in detector counts per second.

In the (224) RSM, the VS signal lies along the line joining the Si(224) peak to the origin, indicating that this material is cubic rather than tetragonal (i.e. that it is fully relaxed) while the Ge peak is found with the same $q_{||}$ as the $Si_{0.2}Ge_{0.8}$ layer, indicating that the Ge QW is lattice-matched to the VS.

2.4.2 Quantum Yield

In bulk Ge, due to the large density of states in the CB, the Fermi level lays very close to the VB even for moderate p-type doping levels ($p \approx 10^{16} - 10^{17}$ cm^{-3}) like those found in the samples under investigation. Moreover, in metal/Ge(001) contacts the Fermi level is pinned very close to the VB band edge [56]. As a consequence, assuming from Ref. 39 a work function $\Phi \approx 1$ eV for the CsO_x layer, the band profile shown by the continuous lines in Fig. 2.6a is obtained for the CsO_x/Ge interface. We notice that, due to the small indirect bandgap of Ge, the bottom of the CB lies always below the vacuum level E_V and NEA conditions cannot be achieved, at variance with larger gap semiconductors, where the CB minima lies above the vacuum level (dashed line in Fig. 2.6a).

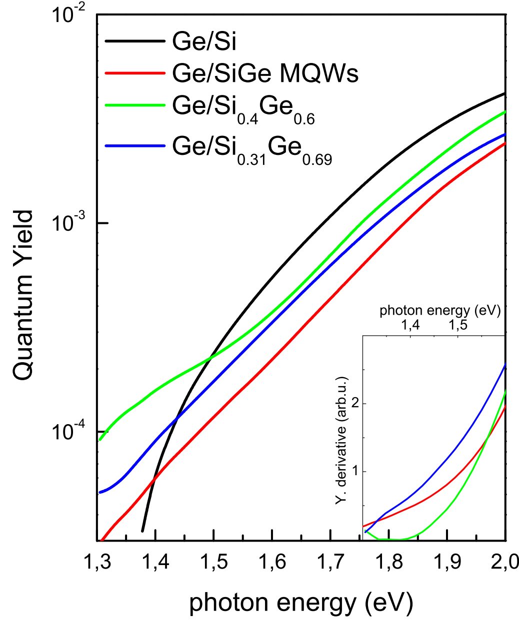

Fig. 2.5: Quantum yield as a function of the exciting photon energy from activated epitaxial Ge/SiGe heterostructures. The spectrum from the 1 μm thick sample (Ge/Si) is in agreement with reported data from bulk Ge photocathodes [39]. The inset shows near threshold derivative spectra from ultrathin films and MQW samples: no structures are detected.

Such dissimilar band profiles are consistent with the two different quantum yield spectra $Y(h\nu)$ observed in III-V compounds and Ge-based photocathodes. Indeed, the photothreshold response for the activated bulk-like sample (#56455), two representative strained thin films (#8491 and #8493), and the MQW sample (#8422) shown in Fig. 2.5 are neither band-gap limited nor proportional to the optical absorption coefficient, as it is instead the case for the NEA photocathodes [3] (see also Fig. 2.3). The positive photoemission barrier present in Ge-based photocathodes acts as an energy filter, so that electrons thermalized in the CB minima are not emitted. This allows to consider for the photoemission process only ballistic electrons originated a few nanometers away from the surface. Note that for NEA photocathodes most of the signal comes instead from electrons thermalized to the bottom of the CB, so that the escape depth is essentially given by the electron diffusion length, which can be of the order of microns [3, 5]. The measured Y values for the Ge-based samples are therefore much smaller

than those achievable in III-V photocathodes [39, 53]. Strained layers are seen to exhibit lower thresholds when compared to the bulk-like epilayer (see Fig. 2.5). Actually for photon energies around 1.3 eV the photoemitted current is seen to monotonically increase with increasing compressive strain. This trend is consistent with a progressive reduction of the photoemission barrier resulting from the bandgap increase induced by compressive strain. The slope change seen in the thin films spectra at photon energies larger than 1.6 eV can be attributed to the onset of substrate emission. Due to its larger direct gap, however, the VS gives no contribution close to threshold. This was experimentally confirmed by performing photoemission experiments on a bare VS with $x = 80$, showing negligible photocurrent for photon energies smaller than 1.8 eV. No clearly resolved structures are present in the $Y(h\nu)$ curves near threshold, as put in better evidence by the very smooth behavior of the derivative curves shown in the inset of Fig. 2.5. The spectrum from the MQW sample #8422 is very similar to the ones from strained films, since, at least in the near threshold region which is the most interesting one when dealing with the electron polarization, most of the signal comes from the 6 nm thick Ge top layer. Therefore no structures are detected, as shown by the derivative curve reported in the inset of Fig. 2.5, differently from the case of III-V based MQW photocathodes, where evident peaks corresponding to transitions between quantum confined states have been observed in the $\mathrm{Y}(h\nu)$ and derivative spectra [10, 57].

2.4.3 Electron Spin Polarization

The relevant energy levels involved in the photoemission process are shown in Fig 2.6b for the case of unstrained and compressively strained ($\varepsilon = -1\%$) Ge. The bandstructure has been obtained by tight-binding calculation [58] and the vacuum-level set at $\mathrm{E}_V \approx 1.0 \pm 0.1$ eV above the VB maximum assuming a Fermi level pinning ≈ 0.1 eV above the VB maximum and using the accurately measured photocurrent data for the CsO_x/Ge(100) surface obtained in Ref. 39. The VB maximum has been chosen as a common reference for a direct comparison of the unstrained and strained case since, neglecting strain-effects on the CsO_x/Ge(100) interface formation, this allows drawing a single E_V level valid for both cases.

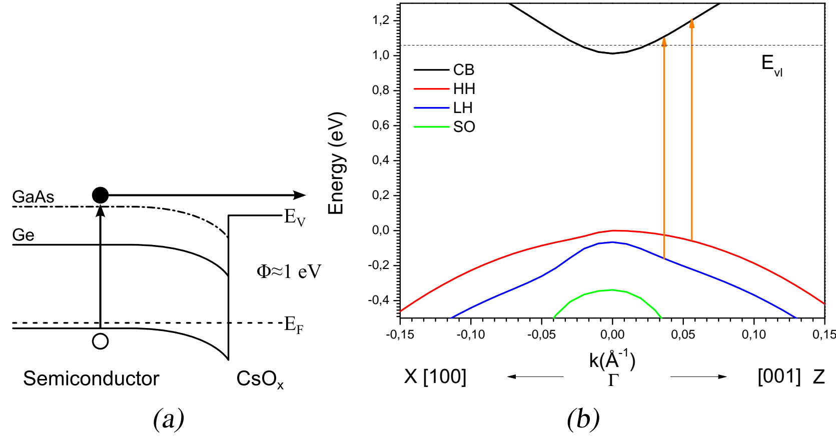

Fig. 2.6: (a) Schematization of the photoemission process. Electrons are excited from VB to CB. In the GaAs case (dot-dashed CB profile) the work function Φ of the cesiated surface is small enough to allow the emission of electrons from the botton of the bulk CB. In case of Ge (continuous CB profile) this is not possible due to its smaller gap. (b) Band structure of Ge around Γ for compressively strained epilayer with strain $\varepsilon = -1\%$. Biaxial compressive strain increases the direct energy gap and removes the degeneracy between HH and LH states at Γ. Arrows indicate transitions for $h\nu = 1.26$ eV.

The two arrows indicate allowed transitions from the HH and LH bands for $h\nu = 1.26$ eV, the minimum photon energy giving reliable spin polarization measurements. From Fig 2.6b it is clear that only VB to CB transitions away from Γ can be probed by photoemission. Optical transitions at Γ have been probed in similar Ge/SiGe MQW samples by absorption [28] and photoluminescence [29] spectroscopy. Electron spin polarization spectra $P(h\nu)$ from most of the samples of Table 2.1 are collected in Fig. 2.7. All spectra present a maximum at threshold and then decrease to zero for larger photon energies, as usual in spin polarized photoemission from semiconductor photocathodes [4,7–13,20,59]. The polarization values from the strained layers are consistently larger than those from the (unstrained) bulk-like sample for excitation energies below ≈ 1.6 eV and above the 50% limit attainable in bulk semiconductors. This can be explained considering that biaxial compressive strain lifts the degeneracy between HH-LH states (see Fig. 2.6b) so that HH-CB transitions, populating only a given spin channel, can be selectively excited without contribution from LH-CB transitions

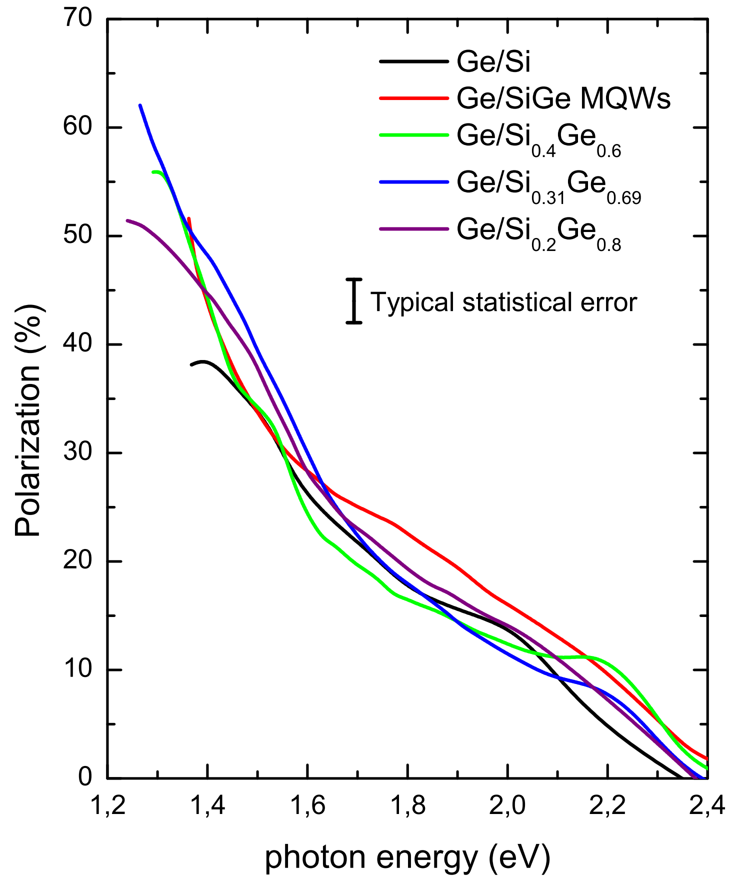

Fig. 2.7: Electron spin polarization as a function of the exciting photon energy from activated epitaxial Ge thin films. The spectrum from the 1μm thick sample (Ge/Si) is in good agreement with reported data from bulk Ge photocathodes [20]. The maximum measured value, P$= 62 \pm 3$%, is well above the 50% limit of bulk systems. Typical statistical error is indicated by the vertical bar. Data taken at T=120 K. Maximum RT values are P$= 40 \pm 3$% and P$= 28 \pm 3$% for the strained and bulk-like samples, respectively.

populating the opposite spin channel. In principle this should lead to a complete polarization of CB electrons, *i.e.* P= 100%: polarizations approaching such value have actually been observed in III-V strained heterostructures under NEA conditions [11, 13]. In our case, even at the lowest photon energy ($h\nu = 1.26$ eV) where Y is sufficiently high ($> 5 \times 10^{-5}$) to assure reliable P measurements, contributions from both HH and LH states are to be expected, as shown by the arrows in Fig. 2.6b, resulting in a reduced P. A similar behavior has been reported also in III-V strained films, where a polarization reduction from values above 80% at threshold to around 60% for photon energies ≈ 100 meV larger than the gap have been observed [11, 13]. A polarization of the order of $30-40\%$, much smaller than the band-gap excitation value, has been predicted in strained/quantum confined Ge structures for non resonant excitation involving both HH-CB and LH-CB transitions [22]. Our results, with polarization values exceeding 60%, well above the 50% limit attainable in bulk semiconductors, indicate that HH-CB transitions predominantly contribute to the photoemitted signal. This suggests that extremely highly polarized electrons can be produced in the CB minimum at Γ also in strained Ge films by using resonant excitation. These electrons cannot however exit the crystal, so that their spin polarization, possibly very high, is not detectable by photoemission but could be revealed by different techniques, such as polarized luminescence [1,2]. Polarized luminescence experiments from quantum confined Ge nanostructures are presently being performed in our laboratories [60]. The effect of compressive strain on the photoelectron polarization is shown in Fig. 2.8, where P values at two different excitation energies, $h\nu = 1.26$ eV and 1.6 eV, are reported as a function of the strain ε present in our films, as measured by HRXRD. The polarization at $h\nu = 1.26$ eV increases starting from the bulk value measured in the 1μm thick film ($\varepsilon = 0$) to a maximum at around $\varepsilon = 1\%$ and then saturates. In a naïve picture, a higher strain should lead to a higher HH-LH splitting and in turn to a higher electron spin polarization. On the other hand, it is known [61] that strain causes a strong intermixing between LH and split-off (SO) states increasing the density of excited electrons with spin opposite to those originating from the HH band and, as consequence, reducing P. Our findings for the dependence of P on ε can then be explained as the results of the competition between the above two mechanisms giving rise to opposite effects.

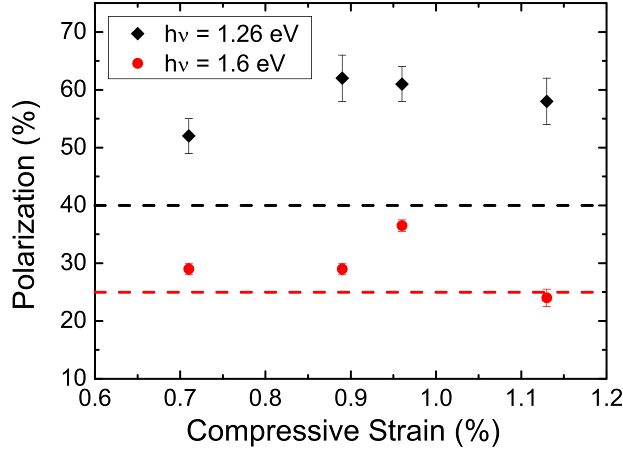

Fig. 2.8: (Colour online) Evolution of the electron spin polarization as a function of compressive strain at $h\nu = 1.26$ eV and 1.6 eV. The two dashed lines indicate the corresponding P measured for the bulk-like Ge.

Finally, we note that in sample #8492 (with a Ge content in the VS $x = 0.5$), the strain relaxation process is more effective and the measured strain level is comparable with that of sample #8509 ($x = 0.8$). In this case, the photoemission yield at threshold is reduced by roughly two orders of magnitude, most probably due to the large number of defects formed during relaxation. In this situation the electron polarization is not detectable because of the unbearable statistical error even though the polarization measured at higher photon energies, where the photoemission signal is stronger, is larger than the corresponding value in bulk Ge.

2.4.4 Valence orbital mixing

Photoemission experiments on strained Ge crystals, performed through Mott polarimetry, have a unique feature that distinguishes them among all the other experimental techniques: it is possible to quantitatively estimate, under proper assumptions that will be explained in the following, the degree of hybridization between valence band states. Referring to Fig. 1.6 and recalling the crystallographic geometry of the analyzed samples, we can argue that the photoemitted electrons have a wave-vector parallel to the [001]-growth direction. In this case the symmetry of the states involved in the transitions, which provides

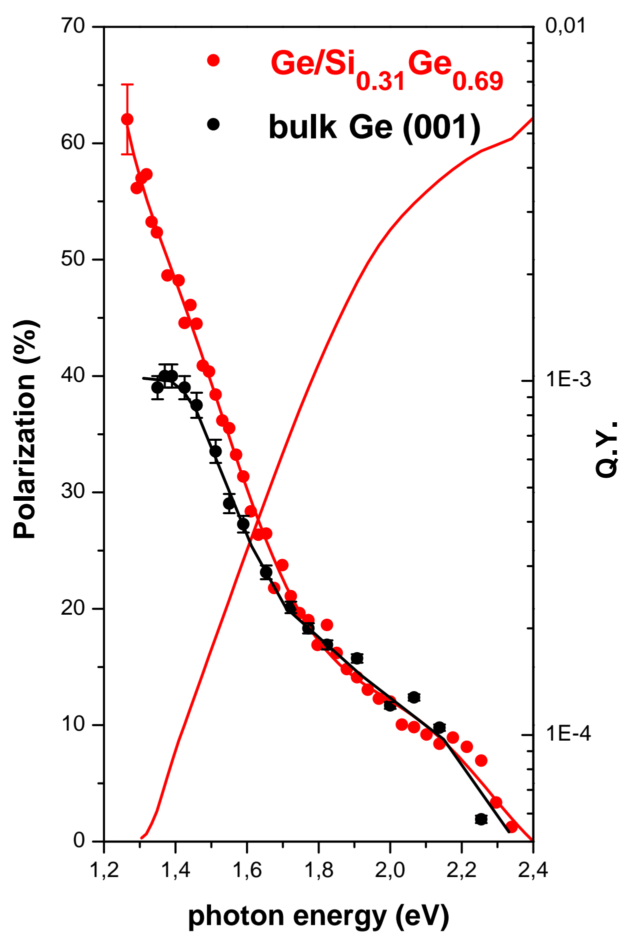

Fig. 2.9: Polarization and Quantum Yield vs. exciting photon energy at T = 120 K for the Ge/$Si_{0.31}Ge_{0.69}$ sample (red dots and line), compared to the P of the thick Ge (001) sample (black dots). The compressive strain induces a net maximum P= 62% which is well above the theoretical limit for bulk structures, *i.e.* P= 50%. Dots represent the experimental points, the red line is obtained through polynomial fitting.

a net P in the conduction band, are the same as in the bulk Ge, as one can see in Fig. 1.6 along the $\Gamma \rightarrow Z$ direction. Thus along the Λ line the states at the bottom of the conduction band will have $\Lambda_7^{2'}$-symmetry, whereas HH, LH and SO states of valence band will belong to Λ_6^5, Λ_7^5 and $\Lambda_7^{2'}$ representations respectively. Due to the fact that the the uncertainty on the vacuum level E_V is greater than the calculated energy difference between HH and LH states at the Γ point, it is reasonable to argue that, similarly to the case of bulk Ge, the photoemission process at $h\nu = 1.26$ eV involves both the Λ_6^5 (HH) and Λ_7^5 (LH) symmetry states. Moreover, we can neglect spin relaxation mechanisms during the transport to the surface of the photoemitted electrons when the excitation energy is $h\nu = 1.26$ eV; such a "ballistic" approximation is still reliable because the time scale of depolarization mechanisms ($\tau = 10^{-11}$ s) is much greater than the characteristic time scale of an excited electron in the conduction band before being emitted in vacuum [2, p.342-343].

Unlike bulk Ge, the in-plane compressive strain increases the energy difference out of the Γ point between HH and LH states. Thus the approximation of quasi-degeneration between these two bands, which is reliable in the proximity of the Γ point in bulk Ge case, cannot be applied in strained Ge layers so that electrons from HH and LH states have considerably different energies when promoted to the conduction band and, consequently, different trasmission coefficients T (see Fig. 2.6b). At this purpose, we can approximate the conduction band as a well, of which the potential V_0 is set by the energy position of the vacuum level E_V. Due to the fact that the position of E_V cannot be measured precisely, we take into account the extreme case whithin our experimental error and we set $E_V = 1.1$ eV. Consequently the height of the well potential, from the bottom of the conduction band, is $V_0 \approx 90$ meV. Then we calculate through standard formula the trasmission coefficient T [62]: when excited with $h\nu =$ 1.26 eV photon energy, electrons from HH and LH bands are promoted in the conduction band with ≈ 90 meV and ≈ 20 meV respectively above E_V and the ratio between the two transmission coefficients is $T_{HH}/T_{LH} \approx 1.15$. Thus the introduction of the mixing coefficient between LH and SO bands found by Allenspach *et al.* for bulk Ge [20], allows a maximum electron spin polarization P$\approx 55\%$. Evidently the result of such a "barrier energy filtering" is not sufficient

alone to explain the experimental result of Fig. 2.9: indeed we shall see that, considering an enhanced strain-related LH-SO orbital mixing, it is possible to obtain the experimental polarization.

Bearing in mind these fundamental assumptions, we focus our attention on the Ge/$Si_{0.31}Ge_{0.69}$ sample of Fig. 2.9: in the proximity of the Γ point we can introduce the treatment developed in Ref. 20 so that the hybridization between valence band states with different orbital symmetry results:

$$\begin{aligned} \Lambda_6^5 &\to \Lambda_6^5 \\ \Lambda_7^5 &\to \Lambda_7^{5,2'} \\ \Lambda_7^{2'} &\to \Lambda_7^{2',5}. \end{aligned} \tag{2.1}$$

If we consider the non-hybridized state of Λ_7^5 symmetry (in the following we shall neglect transition at higher energy) the relative weight of the two different characters in the hybridized wave-functions basically depends on the temperature T, the effective strain degree $\varepsilon_{||}$ of the system and the wave-vector $\mathbf{k}$ involved in the transitions so that:

$$\Lambda_7^{5,2'} = \alpha\left(T,\varepsilon_{||},\mathbf{k}\right)\Lambda_7^5 + \beta\left(T,\varepsilon_{||},\mathbf{k}\right)\Lambda_7^{2'}. \tag{2.2}$$

Considering the experimental data of Fig. 2.9, the maximum P is obtained through the simultaneous transitions from the initial states of Λ_6^5 and $\Lambda_7^{5,2'}$; recalling that transitions $\Lambda_7^{2'} \to \Lambda_7^{2'}$ are forbidden, the intensity related to this dipole transition is removed so that:

$$P(\Lambda) = \frac{1 - 1\cdot|\alpha\left(T,\varepsilon_{||},\mathbf{k}\right)|^2}{1 + |\alpha\left(T,\varepsilon_{||},\mathbf{k}\right)|^2}, \tag{2.3}$$

$$|\alpha\left(T,\varepsilon_{||},\mathbf{k}\right)|^2 + |\beta\left(T,\varepsilon_{||},\mathbf{k}\right)|^2 = 1. \tag{2.4}$$

Thus, considering the experimental value P= 62%, the temperature T = 120 K, a strain coefficient $\varepsilon_{||} = -0.96\%$ and a wave-vector $\mathbf{k}$ in the proximity of the Γ point we have:

$$|\alpha| = 0.48,$$
$$|\beta| = 0.88. \tag{2.5}$$

In this case we have experimentally determined the orbital mixing coefficients between states of Λ_7^5 and $\Lambda_7^{2'}$-symmetry along the Λ line of compressively strained Ge; hereby it is really interesting to note that the $\Lambda_7^{2'}$ character is considerably increased, compared to the case of Δ line in bulk Ge, where $|\beta| \approx 0.82$ [20]. This result can be seemingly considered in contrast with the hybridization coefficient at the Γ point of the Brillouin zone for the tetragonal D_{4h} group: in fact, direct transitions from Γ_6^+ (HH) and Γ_7^+ (LH) symmetry states to the bottom of the conduction band provide in any case a P equal to 50% and mixing coefficient between LH and SO states at $\mathbf{k} = \mathbf{0}$ have to be necessarily equal to those found by Allenspach *et al.* [20]; neverthless in compressively strained Ge the LH band shows an anisotropic dispersion so that along the growth direction (Λ line according to Fig. 1.6) the effective mass heavily decreases in the proximity of the Γ point [63, p. 99], [44–48]. A pictorial behaviour of the strain effect on the valence band around the Γ point can be also appreciated in Fig. 2.10. From a symmetry point of view, it is reasonable to argue that in this case the $\Lambda_7^{2'}$-character of the band increases, so that the hybridization coefficient is slightly enhanced moving away from Γ, to diminish towards the Z point, where the two bands must resemble the bulk-like behaviour. This non-monotonic behaviour of the hybridization between Λ_7^5 and $\Lambda_7^{2'}$ symmetry states, reasonably provides the polarization value, shown in Fig. 2.9.

Eventually, we can also take into account the effect due to the barrier filtering in the conduction band: in this case Eq. 2.3 is slightly modified so that we obtain $\alpha' = 0.52$ and $\beta' = 0.85$, thus showing that the SO-character in LH states is still greater than the one found for bulk Ge in Ref. 20.

We move now to analyze the behaviour of sample 8509 (see Table 2.1): the maximum P is still consistently higher with respect to the bulk sample, but it is lower than the one measured for sample 8493. Indeed the calculated energy difference between HH and LH band at the Γ point is $\Delta E = E_{HH}\text{-}E_{LH} = 43$ meV

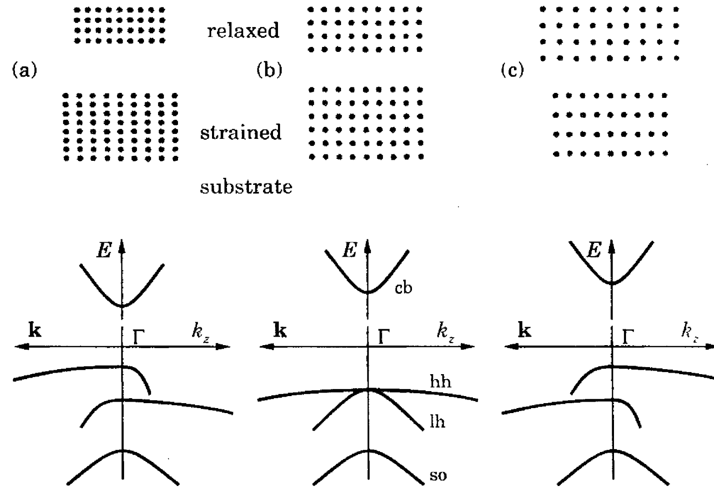

Fig. 2.10: Effect of the strain on the bands of semiconductors around the Γ point for: (a) tensile strain; (b) non strain and (c) compressive strain, which is the proper case for thin Ge films grown on $Si_{1-x}Ge_x$ VS. The compressive strain case (c) shows that LH band has an increased dispersion in the growth direction k_z, which corresponds to Λ line in Fig. 1.6), with respect to the plane where biaxial compressive strain acts ($k_{||}$ or Δ line according to Fig. 1.6) [63].

[61]. For $Ge/Si_{0.2}Ge_{0.8}$ structure, the correction given by the possible presence of the barrier filtering in conduction band is negligible, due to the fact that the direct energy gap E_d diminishes proportionally to the actual degree of the strain but the position of the vacuum level E_V can always be set at ≈ 1.1 eV. Then with the same photon energy $h\nu = 1.26$ eV, we can promote electrons which are not sensibly affected by the presence of a Positive Electron Affinity (PEA). Thus we can try to correlate the hybridization coefficient between Λ_7^5 and $\Lambda_7^{2'}$ symmetry states as function of the strain degree with the same calculation performed in Eqs. 2.4; then we obtain the following results:

$$|\alpha| = 0.57,$$
$$|\beta| = 0.82. \tag{2.6}$$

again for the temperature T = 120 K, an effective strain coefficient $\varepsilon_{||} = -0.82\%$ and a wave-vector **k** in the proximity of the Γ point. Indeed, we can argue that the

hybridization between Λ_7^5 and $\Lambda_7^{2'}$-symmetry states out of the Γ point decreases for a lower strain degree, as expected. Evidently, at this stage it is difficult to correctly determine the behaviour of the orbital mixing coefficient as function of the effective strain: in fact, plastic relaxations do not allow to arbitrarly enhance the effect of the compressive strain and moreover the range of temperature of the measurements above does not provide to directly link these results to those of Ref. 20, being P curves as function of the temperature still lacking for IV group semiconductors.

In conclusion, experimental data on the set of analyzed samples have shown the role of the compressive strain on the Electron Spin Polarization: due to the PEA conditions, the photoemission process takes place out of the Γ point, where the orbital mixing between valence states of Λ_7^5 and $\Lambda_7^{2'}$ symmetry is strong. The anisotropic dispersion of the LH band in the growth direction makes the interaction between these states higher along the Λ line, even though still in the proximity of Γ point, thus increasing the $\Lambda_7^{2'}$- character of $\Lambda_7^{5,2'}$ states: as a consequence the electron spin polarization exceeds the value of 50% even if both Λ_6^5 and $\Lambda_7^{5,2'}$ states are taken into account.

3. SPIN POLARIZED PHOTO-LUMINESCENCE

The following section is devoted to the discussion and analysis of Spin Polarized Photo-Luminescence (SPPL) measurements; indeed this experimental technique can be considered complementary to SPP technique because it allows to detect the electron spin polarization at some points of the Brillouin zone, which are forbidden for Spin Polarized Photoemission. This is especially a crucial advantage when taking into account Ge-based heterostructure where, for example, transition from the valence band to the indirect gap minimum L and the direct gap one Γ, cannot never be detected due to the persistent PEA condition (see Sec. 2.3).

Another important aspect is related to the nature of Photo-Luminescence, which is a photon in-photon out process: as explained in Sec. 2, the photoemission time scale is short enough to neglect possible spin relaxation mechanisms in IV group heterostructures: a SPP spectrum detects only the spin polarization of the electrons which are emitted into the vacuum, being excited at some distance from the Γ point. All the electrons, promoted to the conduction band, which undergo some spin relaxation processes, are eventually scattered to the direct or indirect minimum of the conduction band, thus under the vacuum level. All these information can be provided by SPPL measurements, which detects the P from the recombination of the electrons with holes in the valence band, taking into accout all the spin relaxation mechanisms which involve polarized electrons and also polarized holes. Indeed the knowledge of these phenomena is essential in order to engine IV group-based spintronics devices [64–68]

3.1 Fundamentals of SPPL technique

Spin Polarized Photo-Luminescence relies on the fact that the light, emitted during the recombination between excited electrons in conduction band and holes

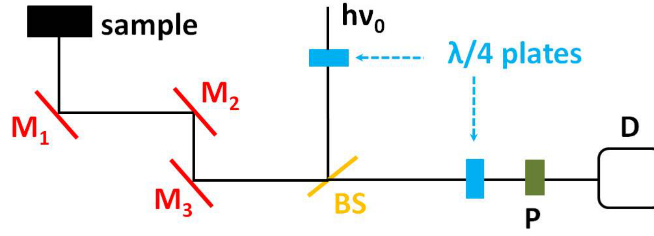

Fig. 3.1: Optical set-up for Spin Polarized Photo-Luminescence measurements: the exciting light of energy $h\nu_0$ is first circularly polarized by $\frac{\lambda}{4}$ retarder and then reflected towards the sample by a beam splitter (BS); three mirrors (M) collect the Luminescence light towards the second $\frac{\lambda}{4}$ retarder, then to the polarized (P) and finally to the InGaAs detector (D).

in the valence band, has a circular polarization degree, which is proportional to the spin polarization of the carriers inside the solid [69]. This basically means that it is possible to deduce the spin-polarization of the carriers through the analysis of the circular polarization of the Luminescence light.

Photoluminescence (PL) measurements has been performed in a back-scattering geometry at 15 K in a closed cycle cryostat. Fig. 3.1 shows the optical set-up which has been employed: a continuous wave (cw) QD laser operating at $h\nu_0 = 1$ eV or a cw Nd-YVO$_4$ laser, operating at $h\nu_0 = 1.16$ eV, were coupled to an optical retarder and used as circularly polarized excitation sources. On the sample, the laser beam has been focused to a spot size of about 100 μm, resulting in an excitation density in the range of $9 \cdot 10^2 - 3 \cdot 10^3\ W/cm^2$. The luminescence polarization has been then probed by a quarter-wave plate followed by a linear polarizer, a long pass filter for the laser line rejection and a spectrometer having a linear dispersion of about 32 nm/mm and equipped with a thermoelectrically-cooled InGaAs array detector. As a check, no circular polarization of the luminescence signal has been detected when exciting with linearly polarized light.

3.2 Experimental results

Two types of samples have been investigated: a Ga doped (p-type) Ge(001) wafer, with doping concentration of N= $3.6 \cdot 10^{18}\ cm^{-3}$ and a Ge/Si$_{0.15}$Ge$_{0.85}$ Multiple Quantum Well (MQW) heterostructure deposited on Si(100). The

deposition of the Ge/$Si_{0.15}Ge_{0.85}$ MQWs has been performed by low-energy plasma-enhanced CVD (LEPECVD). The composition and thickness of the QW and barrier layers have been chosen in such a way that the compressive force acting on the Ge QW is perfectly balanced by the tensile force acting on the $Si_{0.15}Ge_{0.85}$ barriers. In this way, it is possible to deposit several Ge QWs all featuring the same level of compressive strain, which in this case is $\varepsilon_{||} = -0.4$, without inducing any plastic relaxation. Despite the different compressive strain degree, the morphological features of this sample are the same as the MQW sample investigated by SPP, so that for further details the reader can refer to Sec. 2.1.

Let us begin the analysis from the p-doped bulk Ge sample, of which the band structure has already been shown in Fig. 1.2 as well as all the relevant transitions at the Γ point (see Fig. 1.3); in the frame of spherical approximation, the subsystem of interest (with total angular momentum J = 3/2) is suitably described by the effective Luttinger Hamiltonian whose good quantum numbers are the elicity λ and J [70]; on the basis of the helicity operator $\widehat{\lambda}$, for every wave-vector **k**, this kinetic Hamiltonian provides a Kramers doublet with $\lambda = \pm 3/2$ (HH) and $\lambda = \pm 1/2$ (LH) states, conveniently chosen along the propagation direction of the exciting light beam. Conduction band (CB) states at the Γ point are s-like and their total angular momentum is $J = 1/2$ with projection $J_z = \pm 1/2$. As already explained in Sec. 1.1, the maximum theoretical electron spin polarization right after excitation is $P_s = P_s^0 = 50\%$. Here P_s is defined as $P_s = (N^+ - N^-)/(N^+ - N^-)$, where N^+ (N^-) is the number of electrons with spin up (down).

Spin relaxation mechanisms tend to equalize spin up and spin down populations; therefore a steady state condition is reached with $P_s \leq P_s^0$. It should be noted that in our Ge bulk sample the overall hole concentration is not affected by optical excitation of carriers, since, due to the high p-doping level, a Fermi sea of holes with both spins is present no matter the helicity of the excitation. Above all, spin relaxation of holes in bulk material is expected to be much more rapid than for electrons, because of the strong mixing of the HH and LH valence bands [1]. Therefore, even at low temperatures, the photo-created electrons will recombine with non-polarized equilibrium holes.

The degree of the circular polarization of the emitted light, P_c, is defined as $P_c = (I^+ - I^-)/(I^+ - I^-)$, where $I^\pm$ is the intensity of the Photo-Luminescence signal having circular polarization $\sigma^\pm$. P_c is related to the spin polarization P_s through the same matrix elements valid for the absorption process (see Fig. 1.3). Therefore, if no electron spin relaxation occurs and assuming non-polarized holes, the polarization degree of the emitted light is the square of the electron spin polarization in the CB: $P_c^0 = \left(P_s^0\right)^2 = 25\%$ [2, Ch. 2]. Lower values of P_c will be observed when electron spin relaxation mechanism are not negligible. For photoexcitation with circularly polarized light at $h\nu_0 \approx 1$ eV, i.e. with energy between E_d and E_{SO} where E_{SO} is the topmost split-off band energy, the luminescence spectrum in Fig. 3.2a, analyzed for σ^+ (blue curve) and σ^- (orange curve) polarizations, reveals a significant polarization degree $P_c \approx 23\%$. This result demonstrates an electron spin polarization close to its maximum, therefore suggesting that the electron lifetime τ is much shorter than the spin relaxation time, τ_s^e, being $P_c = P_c^0/(1+\tau/\tau_s^e)$ [69]. These findings are in good agreement with reports on direct gap semiconductors such as GaAs [2, Ch. 2] and GaSb [69]. Evidently the simple atomic-like model reported in Fig. 1.3 is not accurate for excitation energies higher than E_d , since for $\mathbf{k} \neq 0$ the identification between HH (LH) and $J_z = \pm 3/2$ ($J_z = \pm 1/2$) states is no longer valid. In addition, Split-Off states can also be excited for photon energies higher than $E_g + E_{SO}$, giving an initial spin polarization lower than 50%. As already demonstrated in bulk GaAs [2, Ch. 2] and predicted in Ge [24], by increasing the excitation energy above the Split-Off threshold, i.e. from $h\nu_0 = 1$ eV to $h\nu_0 = 1.165$ eV, we observed a decrease of the luminescence polarization to $\approx 10\%$, as shown in Fig. 3.2b, which can be explained in terms of the reduced initial spin polarization and/or spin relaxation during electron thermalization [2, Ch. 2]. An accurate determination of the spin-lifetime of electrons distributed within the Γ valley is not straightforward for both the above excitations, due to the lack of data concerning lifetimes for transitions across the direct band-gap of Ge. Nevertheless, we can provide a lower-bound estimate for the spin depolarization time in p-Ge as follows: the observed luminescence from the direct gap can be understood as a result of the recombination of holes with electrons, directly photo-generated within the Γ valley by the laser excitation. The lifetime of such non thermalized

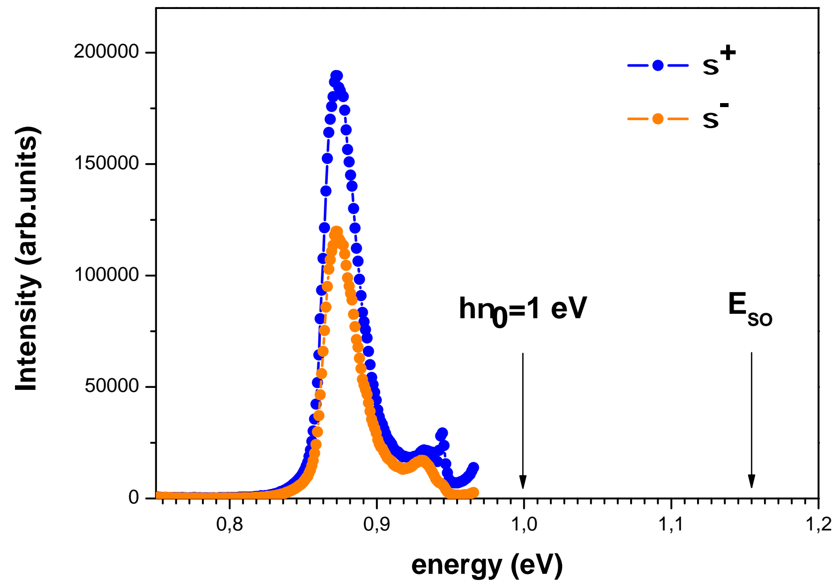

(a)

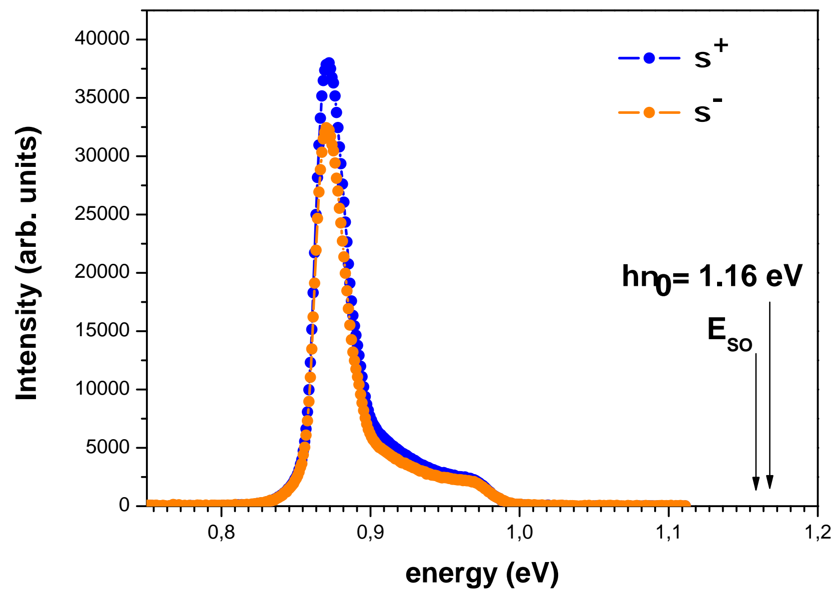

(b)

Fig. 3.2: Spin Polarized Photo-Luminescence spectra at $T = 15$ K of p-doped bulk Ge with two different excitation energies: (a) $h\nu_0 = 1$ eV and $h\nu_0 = 1.165$ eV. The incident exciting light is right-circularly polarized and E_{SO} represents the topmost split-off band energy.

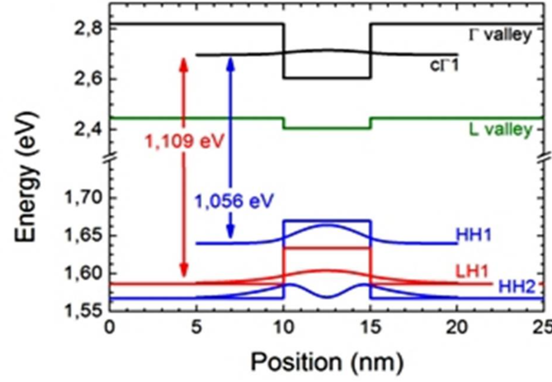

Fig. 3.3: 8-band $k \cdot p$ calculation of the conduction and valence band edge profiles for a Ge well sandwiched in a larger gap barrier material, such as $Si_{0.25}Ge_{0.85}$. Energy levels for the confined states at the Γ point in the conduction band ($c\Gamma n$) and in the valence band, i.e. heavy hole (HHn) and light hole (LHn) states, are reported along with the wavefunction square amplitudes. Dipole allowed transitions associated with the direct-gap electrons (Γ_{7c}) and holes (Γ_{8v}), and their relative energies are also indicated by arrows.

electrons is dominated by the fast $\Gamma - L$ scattering channel. Such mechanism takes place on a 230 fs time scale [71], thus providing a lower-bound estimate for the spin decoherence time. Now let us focus on the MQW sample: Fig. 3.3 summarizes the effects of compressive strain and quantum confinement on the relevant energy levels of Ge as obtained by 8-bands $k \cdot p$ modelling [72]. As also explained in Sec. 1.2, at the top of the valence band the degeneracy between HH and LH states is lifted with the HH laying higher in energy than the LH. At the Γ point the simplified atomic model of electric dipole transition $C\Gamma1$-HH1 with circularly polarized light (Fig. 1.3) predicts $P = 100\%$ and tight-binding calculations [22] confirm this picture for Ge QWs, giving $P_S^0 \approx 96\%$ for the $C\Gamma1$-HH1 transition and values between 28% and 34% away from quantum confined states resonances.

Fig. 3.4 shows the PL spectrum of a Ge MQW structure containing 100 quantum wells 5 nm wide, and 10 nm thick barriers made of $Si_{0.15}Ge_{0.85}$. It should be noted that compared to the emission in bulk Ge, MQW luminescence is blue-shifted because of the combined effect of strain and confinement. As a consequence, due to the close proximity of emission and excitation energies,

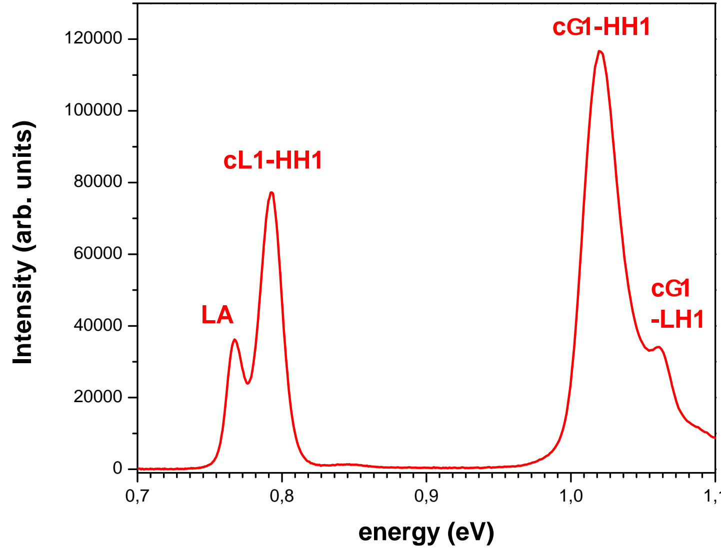

Fig. 3.4: PL emission bands of Ge/SiGe MWQs due to the $c\Gamma1$-HH1 (≈ 1.03 eV), $c\Gamma1$-LH1 (≈ 1.06 eV), cL1-HH1 zero phonon (≈ 0.8 eV) and longitudinal acoustic phonon mediated transitions (≈ 0.77 eV), measured at $T = 15$ K and under 1.165 eV excitation energy.

this sample was investigated only by means of the 1.165 eV laser line. The PL spectrum features can be divided in two groups. The low-energy PL doublet, at ≈ 0.8 eV, can be associated with transitions across the indirect band-gap. In particular, the high energy line is ascribed to the cL1-HH1 recombination or no-phonon emission (NP), while the low energy line of the doublet is the transition mediated by longitudinal acoustic phonons (LA) [28]. It should be noted that, in contrast to the Ge bulk sample, for the MQW sample we have access to the indirect transitions, even though the LA phonon replica might still be affected by the cut-off in sensitivity of the InGaAs detector. The emission band at high energy, ≈ 1.03 eV, is due to the direct gap $c\Gamma1$-HH1 transition between the first electron state in the CB and the first heavy-hole state in VB [28]. By considering the energy level diagram (see Fig. 3.3) and the relative strength of the matrix elements for HH and LH transitions, we can attribute the feature at ≈ 1.06 eV to the $c\Gamma1$-LH1 excitonic recombination, superimposed onto the broad high energy tail of the main $c\Gamma1$-HH1 peak. Fig. 3.5 shows the σ^+ and σ^- luminescence intensity under non-resonant σ^- excitation at $h\nu_0 = 1.165$ eV. The associated polarization degree, P_c, of the $c\Gamma1$-HH1 emission is $P_c = 32\% \pm 5\%$,

well above the maximum theoretical limit of $P_c = 25\%$ achievable in bulk Ge. As already mentioned, with a photon energy of 1.165 eV we excite both the $c\Gamma1$-HH1 and $c\Gamma1$-LH1 transitions. Under this condition and according to calculations in Ref. 22, the initial spin polarization P_s, right after absorption is expected to be comprised between $P_s = 28-34\%$, while the subsequent circular polarization for light emission at the $c\Gamma1$-HH1 transition is about 96% of P_s, finally yielding an expected polarization degree of the luminescence in agreement with our experimental results. Substantially higher values of P_c could be hence achieved for the limiting case of $c\Gamma1$-HH1 resonant- excitation. Such finding demonstrates the effectiveness of strain and quantum confinement effects for the optical control of spin injection in SiGe heterostructures. Heteroepitaxial growth of Ge MQWs therefore provides an effective means to engineer optical injection of spins even in group IV materials, traditionally considered not suitable for optical studies of spin phenomena. The consistency between our spin resolved PL data and calculations concerning electron polarization on Ge/SiGe MQWs of Ref. 22 suggests that after optical orientation electron depolarization mechanisms are negligible even for non-resonant excitation and that heavy holes are equally distributed between their m_j sublevels, i.e. they are completely unpolarized. In particular, the mechanisms leading to the same $|3/2,-3/2\rangle$ and $|3/2,3/2\rangle$ hole populations take place on a time scale which is faster than the electron spin relaxation time despite the decrease in the valence band mixing due to confinement effects. Remarkably, in the $c\Gamma1$-LH1 recombination channel, a clear σ^- contribution is reported, while σ^+ emission is found to be almost missing. By subtracting the broad high energy tail of the HH1 transition we can estimate a polarization degree as high as $\approx 86\% \pm 8\%$: this result strongly suggests that LH are still partially polarized at the moment of electron-hole recombination. After σ^- excitation only $m_j = +1/2$ light holes are created, and since the weak $c\Gamma1$-LH1 $-\sigma^+$ emission is related to $m_s = +1/2$-spin electrons recombining with $m_j = -1/2$ light holes, we must argue that the latter are not sizably present in the sample. Spin polarized PL measurements therefore indicate that photo-generated $|3/2,+1/2\rangle$ holes do not loose their spin orientation, but either recombine radiatively with $|1/2,-1/2\rangle$ electrons, or thermalize their momentum and energy to the HH levels, eventually to the $|3/2,-3/2\rangle$ states via preserving parity scattering events [73]. In this

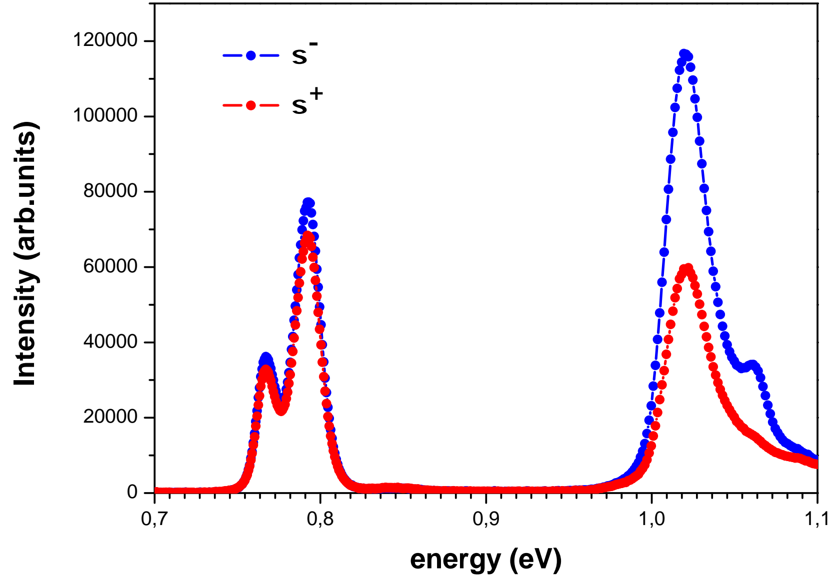

Fig. 3.5: Spin Polarized Photo-Luminescence (SPPL) spectra of Ge/SiGe MQWs, measured at $T = 15$ K and under 1.165 eV excitation energy having a right-hand circular polarization (σ^-). Direct and indirect gap features of the spectrum are resolved for left-hand, σ^- (blue), and right-hand σ^+ (red) circular polarization.

way LH can indeed contribute to counterbalance the $|3/2,3/2\rangle$ hole population produced during the absorption. It is noteworthy that due to the aforementioned cooling process towards HH states at lower energy, which is mainly mediated by acoustic phonon scattering, the lifetime of the LH exciton is expected to be shorter than that of the HH exciton. The different polarization for the $c\Gamma1$-LH1 and $c\Gamma1$-HH1 excitons suggests that the observed spin polarization is determined by the single particle lifetime. Noticeably, in Ge the spin relaxation time of holes, τ_{sh}^h, has to be compared with a mechanism completely absent in III-V compounds, namely electron scattering to the side valleys, τ_e. This phenomenon may have a significant impact on the spin dynamics, since it reduces the permanence of electrons in the Γ region to hundreds of fs and therefore limits the exciton lifetimes [73, 74]. Experimental data for τ_{sh}^h are not yet available even for bulk Ge, but are expected to be in the 0.1-10 ps range [26, 75]. These results suggest that the time needed to equalize the HH population on their m_j sublevels is shorter than $\tau_e \approx 500$ fs [73], whereas the spin relaxation time for LH is larger or at least comparable with the Γ-electron lifetime.

After direct gap excitation at $h\nu_0 = 1.165$ eV, the decay of photo-generated electrons towards the Γ-valley band edge competes with the Γ-L depopulation, which leads to the NP and phonon replica LA emissions. Noticeably, also such indirect transitions are polarized, in particular the NP band at ≈ 792 meV, recorded for both σ^+ and σ^- polarizations reveals a net light polarization degree of about 9% and the LA band displays a polarization degree of about 8%. This is a clear indication that the electron-phonon interaction, responsible for L-valley population, and the subsequent momentum-assisted recombination do not lead to a complete lost of the spin orientation. In this case the evaluation of the electron spin polarization from the measured P_{circ} is much more complicated than in the case of direct transitions, due to the mixed s-p-d nature of the L state [22] and the required momentum transfer. Only very recently such problem has been addressed from a theoretical point of view for phonon assisted transitions in bulk Si [23]. Corresponding calculations are not available for Ge, and, in particular, are missing for the zero-phonon line, which is allowed by small deviations from a non cubic environment associated to interface roughness and strain. The comparison of experimental circular polarization values with future theoretical studies of zero-phonon optical transitions is therefore mandatory to gather access to the spin physics of low dimensional structures based on indirect band-gap materials.

Part II

PROBABILITY-CURRENT AND SPIN-CURRENT IN PRESENCE OF SPIN-ORBIT INTERACTION

3.3 Introduction

The following work is focussed on transport phenomena in presence of Spin- Orbit Interaction (SOI) [76]; evidently semiconductors play a key role in this matter because in this case it is possible to use an approach, close to atomic physics, which relies on the exact knowledge of the electron wave-function. In particular III-V semiconductor compounds are paradigmatic systems to study spin-related transport properties: in fact they do not have bulk inversion asymmetry (T_d-symmetry point group) so that the spin degeneracy is removed by the well known D'yakonov-Perel (DP) field, which has a cubic dependence versus the wave-vector $\mathbf{k}$ [77, 78]. Moreover, in 2D heterostructures, a linear Rashba field [79, p. 178] arises, due to the structural inversion asymmetry [80, 81]. Basically this means that in such compounds, when low dimensional heterostructures are taken into account, the two main SOI terms can be studied so that III-V semiconductor compounds, like GaAs, result really appealing to study spin-related properties of charge particles.

Evidently the two relevant quantities for transport phenomena are the probability- current and the spin-current; the probability current is a fundamental concept in quantum mechanics, which connects the wave-like description of a quasi-particle to the notion of transport current. When a general Schrödinger problem is considered, the Hamiltonian is

$$\widehat{H}_0 = \frac{\widehat{\mathbf{p}}^2}{2m} + \mathfrak{U}(\mathbf{r}), \tag{3.1}$$

where the real potential $\mathfrak{U}(\mathbf{r})$ is periodic in a crystalline solid and m is the free-electron mass; in this case one is led to the usual definition of free-electron current probability [82, p. 238]:

$$\mathbf{J}^f[\psi] = \mathrm{Re}\left[\psi^* \frac{\hat{\mathbf{p}}}{m}\psi\right] = \frac{\hbar}{m}\mathrm{Im}\left[\psi^* \nabla\psi\right]. \tag{3.2}$$

However, in condensed-matter systems in the presence of Spin-Orbit Interaction (SOI), the potential is no longer real so that a redefinition of this quantity is mandatory. A debated example of this subtle point is provided by semiconductors-

based systems, whose proper treatment requires consideration of the Hamiltonian

$$\widehat{H} = \widehat{H}_0 + \widehat{H}_{SO} \tag{3.3}$$

with

$$\widehat{H}_{SO} = \frac{\hbar}{4m^2c^2} \left(\nabla \mathfrak{U} \times \hat{\mathbf{p}}\right) \cdot \hat{\sigma}. \tag{3.4}$$

Due to the fact that SOI terms in the Hamiltonian have a dependence with respect to the power of the momentum operator $\hat{\mathbf{p}}$, it is reasonable to express the full Hamiltonian, involving SOI terms, as an effective Hamiltonian which consists of momentum-operator $\hat{\mathbf{p}}$-power series expansion, as already shown by Hoai Nguyen *et al.* [83]: indeed, beside the kinetic energy, quadratic in $\hat{\mathbf{p}}$, the SOI provides leading terms that are linear and cubic in $\hat{\mathbf{p}}$, known respectively as Rashba [79] and D'yakonov-Perel (DP) [77, 78] terms. Then, since the SOI potential is non real, a more general definition of the probability current $\mathbf{J}[\psi]$ has necessarily to be taken into account. Considering interactions that include higher-order polynomial terms in the Hamiltonian, we have to deal with an effective Hamiltonian of order n.

Furthermore, an open question, strictly linked to the one above, concerns the definition of spin current (SC). Indeed, in semiconductor physics, that provides paradigmatic systems for spintronics, it is known that the SC standard definition, used by many authors [84–89], can be suitably applied to two dimensional (2D) systems with Rashba SOI, but fails to describe spin-dependent transport phenomena in bulk cubic semiconductors, where SOI induces a DP term in the conduction band. The existence of extra-current terms was also pointed out in Ref. 90. Drouhin *et al.* [91] have shown that a redefinition of SC is mandatory to obtain a unified treatment, enlightening the fact that a properly-symmetrized spin-current operator $\hat{\mathbf{J}}_{\uparrow(\downarrow)}[\psi]$, where $\uparrow$ $(\downarrow)$ refers to up (down) spin channel, gives unexpected results when applied to tunneling through evanescent states in GaAs barriers.

As pointed out by Rashba in Ref. 85, there are still concerns relying on the fact that a consistent theory of spin transport currents has not been formulated yet. From a general point of view, it means that we cannot immediately approach such a topic in terms of non equilibrium thermodynamics. In fact, a difficulty relies

on the definition of system in order to formulate relevant balance equations and also on the boundary terms which should possibly be included in the effective Hamiltonian. Recently, Shi *et al.* [92] have proposed an alternative spin-current operator, satisfying the continuity equation, that allegedly supports important conclusions concerning conservation of spin currents [93–95], but which appears to rely on non-explicit assumptions (see Sec. 4).

The inclusion of SOI in the Hamiltonian of a system has direct and practical consequences in heterostructures, where a consistent analysis of the tunneling phenomena is required. The pragmatic BenDaniel-Duke (BDD) approach [96], that perfectly works when dealing with quadratic Hamiltonians under effective-mass approximation, cannot be straightforwardly extended because it is not always possible to ensure both the continuity of the envelope function and the conservation of the probability current, which is mandatory under steady-state conditions. Then it is necessary to revisit both the probability-current expression and the boundary conditions. This is in line with the ideas of Harrison [97].

In this chapter, a systematic construction of the probability-current operator $\hat{\mathbf{J}}$ is presented, which is based on an effective Hamiltonian written as a $\hat{\mathbf{p}}$-power series expansion. The relation between the velocity operator and the current operator, evidencing the simple structure of the extra terms will be analyzed to yield easy and compact calculations whereas explicit treatments in particular cases resulted in lengthy calculations [90]. This novel current operator can be subsequently used to build the SC operators according to the procedure described in Ref. 91. Then, the proper of an hereostructure interface is studied, in order to introduce proper matching conditions at the boundaries, which generalize the BDD procedure, the simplest efficient way to deal with semiconductor heterostructures. Finally, this method is applied on three examples: the case of a quadratic Hamiltonian, where we recover the usual situation (continuity of the envelope function and of the velocity), the case where a Rashba term is added as a perturbation to the BDD Hamiltonian (there we find that the envelope function is continuous, but its derivative is discontinuous), and the case where a cubic DP term is added to the BDD Hamiltonian (where we prove that the envelope function cannot be continuous).

The layout of the chapter is as follows: Sec. 4 is devoted to a general

construction of current operators and a derivation of local properties. In Sec. 5, a general Hamiltonian $\hat{H}^{(n)}$ is introduced as n^{th}-degree homogenous function of momentum-operator coordinates with the subsequent derivation of the velocity operator; moreover it is shown that a proper symmetrization yields the Hermitian current operator $\widehat{\mathbf{J}}$. Sec. 5.4, boundary conditions which are suitable to deal with heterostructures, are proposed and in Sec. 5.5, they are applied to electron tunneling through a $[110]$-oriented GaAs barrier. Finally, in Sec. 5.6, the problem of the spin-current definition will be taken into accout in order to show how to extend the construction procedure to the spin current operators. For further information the reader can refer to Ref. 76, 98.

4. GENERAL DEFINITION OF CURRENT OPERATORS

A difficulty, that arises when a current operator is taken into account, relies on the correct definition of the system and of its boundaries: in fact, considering the density ρ of a physical quantity, we need to satisfy the continuity equation of $\mathbf{J}$, defining a source term G, so that:

$$\frac{\partial \rho}{\partial t} + \nabla \cdot \mathbf{J} = G. \tag{4.1}$$

As pointed out in Ref. 92, the continuity of $\mathbf{J}$ can be ensured by introducing a general source term G, as in Eq. 4.1, but the source term is not uniquely defined and this leads to possible confusion when considering the conservation laws in terms of non-equilibrium thermodynamic equations. In fact, a thermodynamic model only based on the continuity equation Eq. 4.1 cannot take into account the exchange of energy e with the environment introduced by the current generator and the spin-orbit interaction. Indeed, the consequence of the Gibbs equation

$$\frac{de}{dt} = T\frac{\partial s}{\partial t} + \mu\frac{\partial \rho}{\partial t} \tag{4.2}$$

where s is the entropy, T the temperature, and μ is the chemical potential, is that the continuity equation of the density of carriers ρ is necessarily determined by the power dissipated at the boundaries. At zero temperature, the source term is equal to the power dissipated divided by the chemical potential $\partial\rho/\partial t = (1/\mu)\mathrm{d}e/\mathrm{d}t$. This is the reason why the decomposition between the divergence term and the source term G cannot be unique without specifying the boundary conditions. In any case, we first need to state clearly the local properties of a current operator, postponing the analysis of its global properties. For this purpose, we consider a linear operator $\widehat{A}$ that does not explicitly depend on

time and acts over a generic state ψ. In the following we adopt the notation $\left(\widehat{A}\right) = \left(\psi \middle| \widehat{A}\psi\right) = \psi^\dagger \widehat{A}\psi$ used in Ref. 83. The general Schrödinger problem reads:

$$i\hbar\frac{\partial}{\partial t}\psi = \widehat{\mathcal{H}}\psi \tag{4.3}$$

where $\widehat{\mathcal{H}}$ may be any Hamiltonian. For example $\widehat{\mathcal{H}}$ may be equal to $\widehat{H}$ (defined in Eq. 3.3) or to $\widehat{H}_{eff}$ (defined below in Eq. 5.1). We explicitly develop the derivative of $\widehat{A}$ with respect to time:

$$\frac{\partial}{\partial t}\left(\widehat{A}\right) = \frac{\partial}{\partial t}\left(\psi^\dagger \widehat{A}\psi\right) = \frac{\partial}{\partial t}\left(\psi^\dagger\right)\widehat{A}\psi + \psi^\dagger\widehat{A}\left(\frac{\partial}{\partial t}\psi\right) \tag{4.4}$$

and with the help of Eq. 4.3 we obtain:

$$\frac{\partial}{\partial t}\left(\widehat{A}\right) = -\frac{1}{i\hbar}\left(\widehat{\mathcal{H}}\psi\right)^\dagger\widehat{A}\psi + \frac{1}{i\hbar}\psi^\dagger\widehat{A}\left(\widehat{\mathcal{H}}\psi\right) = \frac{1}{i\hbar}\left[\psi^\dagger\widehat{A}\widehat{\mathcal{H}}\psi - \left(\widehat{\mathcal{H}}\psi\right)^\dagger\widehat{A}\psi\right]. \tag{4.5}$$

If $\widehat{A}$ is an Hermitian *matrix* (the elements of which are complex numbers, not differential operators)

$$\left(\widehat{\mathcal{H}}\psi\right)^\dagger\widehat{A}\psi = \left(\psi^\dagger\widehat{A}\widehat{\mathcal{H}}\psi\right)^*, \tag{4.6}$$

so that we can rewrite Eq. 4.5 in a more suitable way that we refer to as the local form of Ehrenfest theorem:

$$\frac{\partial}{\partial t}\left(\widehat{A}\right) = \frac{2}{\hbar}\mathrm{Im}\left(\psi^\dagger\widehat{A}\widehat{\mathcal{H}}\psi\right). \tag{4.7}$$

The integration over the whole space leads to the well known Ehrenfest's theorem, whose global form is valid for any (possibly differential) Hermitian operator $\widehat{A}$:

$$\frac{\partial}{\partial t}\left\langle\widehat{A}\right\rangle = \frac{1}{i\hbar}\left[\left\langle\psi\middle|\widehat{A}\widehat{\mathcal{H}}\middle|\psi\right\rangle - \left\langle\widehat{\mathcal{H}}\psi\middle|\widehat{A}\middle|\psi\right\rangle\right] = \frac{1}{i\hbar}\left\langle\psi\middle|\left[\widehat{A},\widehat{\mathcal{H}}\right]\middle|\psi\right\rangle. \tag{4.8}$$

We can write

$$\frac{\partial}{\partial t}\left(\widehat{A}\right) = \frac{1}{\hbar}\mathrm{Im}\left(\psi^\dagger\left\{\widehat{A},\widehat{\mathcal{H}}\right\}\psi\right) + \frac{1}{\hbar}\mathrm{Im}\left(\psi^\dagger\left[\widehat{A},\widehat{\mathcal{H}}\right]\psi\right) \tag{4.9}$$

with $\left\{\widehat{a},\widehat{b}\right\} = \widehat{a}\widehat{b}+\widehat{b}\widehat{a}$, and, by integration over the whole space, we get

$$\int \mathrm{d}^3r \mathrm{Im}\left(\psi^\dagger \left\{\widehat{A},\widehat{\mathcal{H}}\right\}\psi\right) = 0. \tag{4.10}$$

The time derivative of $\left(\widehat{A}\right)$ is composed of two parts, concerning two different physical processes: we respectively recognize in Eq. 4.9 the divergence of the current and the source term G associated to $\widehat{A}$

$$\nabla\cdot\mathbf{J}_A = -\frac{1}{\hbar}\mathrm{Im}\left(\psi^\dagger \left\{\widehat{A},\widehat{\mathcal{H}}\right\}\psi\right) = -\frac{1}{\hbar}\mathrm{Im}\left(\psi^\dagger \left\{\widehat{A},\widehat{\mathcal{H}}-\mathcal{U}\right\}\psi\right), \tag{4.11}$$

where any real potential $\mathcal{U}$ vanishes when taking the imaginary part of the anticommutator, and

$$G = \frac{1}{\hbar}\mathrm{Im}\left(\psi^\dagger \left[\widehat{A},\widehat{\mathcal{H}}\right]\psi\right). \tag{4.12}$$

The above procedure has two advantages: first, we have expressed in a general form all the quantities entering Eq. 4.1 through commutators and anticommutators; then we have related the probability-current expression directly to the local properties of its corresponding operator, without taking into account a closed system (such a procedure does not automatically imply that the integral of $\nabla\cdot\mathbf{J}_A$ over the crystal only is zero). The choice of considering open systems makes the current operator involve Dirac distributions to deal properly with possible discontinuities at the boundaries of a subsystem. It has to be noted that it is always possible to include the source G term in the form of a current $\mathbf{J}_G$, $G=\nabla\cdot\mathbf{J}_G$ so that the conservation equation becomes

$$\frac{\partial}{\partial t}\left(\widehat{A}\right) + \nabla\cdot\left(\mathbf{J}_A-\mathbf{J}_G\right) = \frac{\partial}{\partial t}\left(\widehat{A}\right) + \nabla\cdot\mathcal{J}=0 \tag{4.13}$$

where $\mathcal{J} = \mathbf{J}_A-\mathbf{J}_G$ is divergence-free in steady-state regime. For instance, if we look for $\mathbf{J_G} = \nabla U_G$, the potential U_G is a solution of the Laplacian problem $\Delta U_G = G$. Moreover, adding to $\mathbf{J}_G$ the term $\nabla\times\mathcal{A}_G$, where $\mathcal{A}_G$ is an arbitrary vector field, does not affect the conservation equation. At this stage, the boundary conditions are not under control. In Ref. 92 the authors observe that it might often

happen that

$$\int_{\mathbb{V}} \mathrm{d}^3 r\, G = 0 \tag{4.14}$$

where the integration is performed over the volume of the system $(\mathbb{V})$. Then

$$\int_{\mathbb{V}} \mathrm{d}^3 r\, G = \int_{\mathbb{V}} \mathrm{d}^3 r\, \nabla \cdot \mathbf{J}_G = \int_{\mathbb{S}} \mathbf{J}_G \cdot \mathrm{d}\mathbf{s} = 0 \tag{4.15}$$

where the volume integral is changed into a surface integral through Ostrogradski's theorem (here $\mathbb{S}$ is the surface limiting $\mathbb{V}$ and $\mathrm{d}\mathbf{s}$ is the surface element along the normal to $\mathbb{S}$). Such a relation is obviously satisfied provided that $\mathbf{J}_G \cdot \mathrm{d}\mathbf{s} = 0$, i.e., provided that $\mathbf{J}_G$ is a tangential vector to $\mathbb{S}$, which is "physically" reasonable. Moreover one can further assume, as reported in Ref. 92 that $\mathbf{J_G}$ "is a material property that should vanish outside the sample": this is a more restrictive and questionable hypothesis. For instance in the case of a magnetic field, the effect of the associated vector potential cannot *a priori* be overlooked outside the sample. Anyway, let us assume that $\mathbf{J_G} = \mathbf{0}$ at the surface $\mathbb{S}$. In this case it is straightforward to show, after partial integration where the boundary contribution cancels, that

$$\int \mathrm{d}y\, \mathrm{d}z\, \mathrm{d}x\, x \left(\frac{\partial J_{G,x}}{\partial x} + \frac{\partial J_{G,y}}{\partial y} + \frac{\partial J_{G,z}}{\partial z} \right) = -\int \mathrm{d}^3 r\, J_{G,x} \tag{4.16}$$

where $J_{G,x}$, $J_{G,y}$, and $J_{G,z}$ are the Cartesian components of $\mathbf{J_G}$. Then

$$\begin{aligned} \int \mathrm{d}^3 r\, \mathbf{J}_G &= -\int \mathrm{d}^3 r\, \mathbf{r} \nabla \cdot \mathbf{J}_G = -\int \mathrm{d}^3 r\, \mathbf{r} G \\ &= -\frac{1}{\hbar} \int \mathrm{d}^3 r\, \mathbf{r}\, \mathrm{Im} \left(\psi^\dagger \left[\widehat{A}, \widehat{\mathcal{H}} \right] \psi \right) = -\frac{1}{\hbar} \int \mathrm{d}^3 r\, \mathrm{Im} \left(\psi^\dagger \mathbf{r} \left[\widehat{A}, \widehat{\mathcal{H}} \right] \psi \right). \end{aligned} \tag{4.17}$$

It is easy to check that, provided that $\left[\widehat{A}, \mathbf{r} \right] = 0$,

$$\mathbf{r} \left[\widehat{A}, \widehat{\mathcal{H}} \right] = \left[\widehat{A}\mathbf{r}, \widehat{\mathcal{H}} \right] - i\hbar \widehat{v} \widehat{A}, \tag{4.18}$$

where $\left[\mathbf{r},\widehat{\mathcal{H}}\right]=i\hbar\widehat{v}$. Thus

$$\begin{aligned}\int \mathrm{d}^3r\,\mathbf{J}_G &= -\frac{1}{\hbar}\int \mathrm{d}^3r\,\mathrm{Im}\left(\psi^\dagger\left[\widehat{A}\mathbf{r},\widehat{\mathcal{H}}\right]\psi\right)+\int \mathrm{d}^3r\,\mathrm{Re}\left(\psi^\dagger\widehat{v}\widehat{A}\psi\right)\\ &= -\frac{1}{\hbar}\int \mathrm{d}^3r\,\mathrm{Im}\left(\psi^\dagger\left[\widehat{A}\mathbf{r},\widehat{\mathcal{H}}\right]\psi\right)+\int \mathrm{d}^3r\,\widetilde{\mathbf{J}}_A. \end{aligned}\tag{4.19}$$

Here, $\widetilde{\mathbf{J}}_A$ is the canonical current defined as

$$\widetilde{\mathbf{J}}_A=\mathrm{Re}\left(\psi^\dagger\,\widehat{v}\widehat{A}\,\psi\right)=\psi^\dagger\frac{\widehat{v}\widehat{A}+\widehat{A}\,\widehat{v}}{2}\psi. \tag{4.20}$$

According to Eq. 4.5, we can write

$$\int \mathrm{d}^3r\,\mathbf{J}_G=-\int \mathrm{d}^3r\,\left[\frac{\mathrm{d}\left(\widehat{A}\mathbf{r}\right)}{\mathrm{d}t}-\widetilde{\mathbf{J}}_A\right]=\int \mathrm{d}^3r\,\left[\widetilde{\mathbf{J}}_A-\frac{\mathrm{d}\left(\widehat{A}\mathbf{r}\right)}{\mathrm{d}t}\right]. \tag{4.21}$$

In Ref. 92 the *effective* current density is defined as $\overline{\mathbf{J}}_G$

$$\overline{\mathbf{J}}_G=\widetilde{\mathbf{J}}_A-\frac{\mathrm{d}\left(\widehat{A}\mathbf{r}\right)}{\mathrm{d}t}.$$

We have the two following relations which define respectively the total current $\mathcal{J}$ and the *effective* total current $\overline{\mathcal{J}}$

$$\mathcal{J} = \mathbf{J}_A-\mathbf{J}_G, \tag{4.22a}$$

$$\overline{\mathcal{J}} = \mathbf{J}_A-\overline{\mathbf{J}}_G=\frac{\mathrm{d}\left(\widehat{A}\mathbf{r}\right)}{\mathrm{d}t}+\left(\mathbf{J}_A-\widetilde{\mathbf{J}}_A\right). \tag{4.22b}$$

Provided $\mathbf{J}_A-\widetilde{\mathbf{J}}_A=0$, i.e. when making the confusion between the canonical and the true currents (which is justified only for Hamiltonians up to second order in $\widehat{\mathbf{p}}$, see Sec. 5), the effective total current becomes $\overline{\mathcal{J}}=\mathrm{d}\left(\widehat{A}\mathbf{r}\right)/\mathrm{d}t$, which is Eq. 5 in the papers by Shi et al. [92] and also by Zhang et al., [94] and is the cornerstone of their further calculations. After a careful analysis, this relation appears to be derived under very special conditions so that it cannot be general. Moreover, the meaning of the so-called effective currents and their relationship with the true

currents are not clear. Their use to tackle local transport equations is not justified.

In Eq. 4.7, we derived the local form of the Ehrenfest theorem for a general operator $\widehat{A}$ and deduced the expression of the associated current $\mathbf{J}_A$. First, consider the case where $\widehat{A}=\widehat{I}$, where $\widehat{I}$ is the identity and the quadratic Hamiltonian $\widehat{\mathbf{p}}^2/2m$. We rewrite Eq. 4.7 as

$$\frac{\partial}{\partial t}|\psi|^2 = -\nabla\cdot\mathrm{Re}\left(\psi^\dagger\frac{\widehat{\mathbf{p}}}{m}\psi\right) = -\nabla\cdot\mathbf{J}[\psi] \tag{4.23}$$

We recover the usual expression for the free-electron probability current

$$\mathbf{J}[\psi] = \mathrm{Re}\left(\psi^\dagger\frac{\widehat{\mathbf{p}}}{m}\psi\right). \tag{4.24}$$

Note that:

$$\begin{aligned}\frac{\partial}{\partial t}|\psi|^2 &= \frac{1}{i\hbar}\left[\left(\psi^\dagger\frac{\widehat{\mathbf{p}}^2}{2m}\psi\right) - \left(\psi^\dagger\frac{\widehat{\mathbf{p}}^2}{2m}\psi\right)^*\right]\\ &= \frac{1}{i\hbar}\left[\left(\psi^\dagger\frac{\widehat{\mathbf{p}}^2}{2m}\psi\right) - \left(\widehat{K}_0\psi\right)^\dagger\frac{\widehat{\mathbf{p}}^2}{2m}\left(\widehat{K}_0\psi\right)\right]\end{aligned} \tag{4.25}$$

where $\widehat{K}_0$ is the time-reversal Kramers operator for a spinless particle, which consists of taking the complex conjugate in the $\mathbf{r}$-representation. Let us check the expression of the current operators we defined under time inversion symmetry. For this purpose we consider the term

$$\begin{aligned}-2i\hbar\nabla\cdot\mathbf{J}_A &= 2i\mathrm{Im}\left(\psi^\dagger\left\{\widehat{A},\widehat{H}\right\}\psi\right)\\ &= \left[\psi^\dagger\widehat{A}\widehat{H}\psi - \left(\psi^\dagger\widehat{A}\widehat{H}\psi\right)^*\right] + \left[\psi^\dagger\widehat{H}\widehat{A}\psi - \left(\psi^\dagger\widehat{H}\widehat{A}\psi\right)^*\right].\end{aligned} \tag{4.26}$$

First, look at the term $\psi^\dagger\widehat{A}\widehat{H}\psi$

$$\begin{aligned}\left(\widehat{K}\psi\middle|\widehat{A}\widehat{H}\widehat{K}\psi\right) &= \left(\widehat{K}_0\psi\middle|\widehat{R}^\dagger\widehat{A}\widehat{H}\widehat{K}\psi\right)\\ &= \left(\widehat{K}_0\psi\middle|\widehat{R}^\dagger\widehat{A}\widehat{K}\widehat{H}\psi\right) = -\varepsilon_A\left(\widehat{K}_0\psi\middle|\widehat{R}^\dagger\widehat{K}\widehat{A}\widehat{H}\psi\right)\\ &= -\varepsilon_A\left(\widehat{K}_0\psi\middle|\widehat{K}_0\widehat{A}\widehat{H}\psi\right) = -\varepsilon_A\left(\psi\middle|\widehat{A}\widehat{H}\psi\right)^*\end{aligned} \tag{4.27}$$

Here, $\widehat{K} = \widehat{R}\widehat{K}_0$ is the Kramers operator for a particle with spin $1/2$, $\widehat{R} = -i\sigma_y$ $\left(\widehat{R}^\dagger = \widehat{R}^{-1}\right)$, and $\varepsilon_A = \pm 1$ depending wether $\widehat{A}$ verifies [99, p. 675]

$$\widehat{K}\widehat{A}\widehat{K} = \varepsilon_A \widehat{A} \quad \text{or} \quad \widehat{R}^\dagger \widehat{A}\widehat{R} = \varepsilon_A \widehat{A}^*. \tag{4.28}$$

Similarly, for the term $\psi^\dagger \widehat{H}\widehat{A}\psi$

$$\begin{aligned}\left(\widehat{K}\psi \middle| \widehat{H}\widehat{A}\widehat{K}\psi\right) &= -\varepsilon_A \left(\widehat{K}_0\psi \middle| \widehat{R}^\dagger \widehat{K}\widehat{H}\widehat{A}\psi\right) \\ &= -\varepsilon_A \left(\widehat{K}_0\psi \middle| \widehat{K}_0\widehat{H}\widehat{A}\psi\right) = -\varepsilon_A \left(\psi \middle| \widehat{H}\widehat{A}\psi\right)^*. \end{aligned} \tag{4.29}$$

Thus, we obtain

$$2i\mathrm{Im}\left(\psi^\dagger \left\{\widehat{A},\widehat{H}\right\}\psi\right) = \psi^\dagger \left\{\widehat{A},\widehat{H}\right\}\psi + \varepsilon_A \left(\widehat{K}\psi\right)^\dagger \left\{\widehat{A},\widehat{H}\right\}\left(\widehat{K}\psi\right). \tag{4.30}$$

We conclude that the general expression for the current of $\widehat{A}$ is

$$\nabla\cdot\mathbf{J}_A = -\frac{1}{2i\hbar}\left[\psi^\dagger \left\{\widehat{A},\widehat{H}\right\}\psi + \varepsilon_A \left(\widehat{K}\psi\right)^\dagger \left\{\widehat{A},\widehat{H}\right\}\left(\widehat{K}\psi\right)\right]. \tag{4.31}$$

5. PROBABILITY CURRENT OF AN EFFECTIVE HAMILTONIAN

5.1 Formulation of the general n^{th}-order Hamiltonian

Considering *effective* Hamiltonians, we deal with general expressions given by momentum series expansions, i.e., constructed from the energy expressed as wave-vector-component series expansion after the substitution $\{k \longrightarrow -i\nabla\}$. We write the effective Hamiltonian $\widehat{H}_{eff}$ as follows:

$$\widehat{H}_{eff} = \widehat{H}_{\mathbf{p}} + V(\mathbf{r}) \tag{5.1}$$

where $V(\mathbf{r})$ is a potential which may be the potential of a single barrier or the one of a superlattice, for example, $\widehat{H}_{\mathbf{p}}$ is such that

$$\widehat{H}_{\mathbf{p}} = \sum_n \sum_{\substack{l(k)\in\{x,y,z\} \\ k=1,\dots,n}} c_{l(1),l(2),\cdots,l(n)} \widehat{p}_{l(1)} \cdots \widehat{p}_{l(n)} = \sum_n \widehat{H}^{(n)} \tag{5.2}$$

where $\widehat{p}_{l(k)}$ is the momentum operator associated to the $l(k)$ Cartesian coordinate and where $c_{l(1),\cdots,l(n)}$ are Hermitian matrices which are invariant under permutation of the subscripts. The abstract form of Eq. 5.2 allows us to perform easy calculations. In Sec. 5.2 we show how to handle such a general expression to deal with concrete situations.

Formally, we perform the identification

$$\underbrace{c_x \dots c_x}_{\alpha} \underbrace{c_y \dots c_y}_{\beta} \underbrace{c_z \dots c_z}_{\gamma} = c_{\underbrace{x \dots x}_{\alpha}, \underbrace{y \dots y}_{\beta}, \underbrace{z \dots z}_{\gamma}} \tag{5.3}$$

where α, β, and γ are integers. We obtain

$$\widehat{H}^{(n)} = (c_x\widehat{p}_x + c_y\widehat{p}_y + c_z\widehat{p}_z)^n . \tag{5.4}$$

Given Eqs. 5.2, 5.3, and 5.4, let us note that only terms such as c_{xx} or c_{xy} (for $n = 2$) are meaningful, a term such as c_x being only a trick in the calculation.

Alternatively, one can write

$$\widehat{H}^{(n)} = \sum_{\alpha+\beta+\gamma=n} c^{\alpha\beta\gamma}\, \widehat{p}_x^{\alpha}\, \widehat{p}_y^{\beta}\, \widehat{p}_z^{\gamma} \tag{5.5}$$

with

$$c^{\alpha\beta\gamma} = \frac{n!}{\alpha!\beta!\gamma!} c_x^{\alpha} c_y^{\beta} c_z^{\gamma} \tag{5.6}$$

We are now in a position to tackle the problem of velocity, first when the Hamiltonian $\widehat{H}$ takes into account the SOI, and, second, when the Hamiltonian $\widehat{H}_{eff}$ is an effective Hamiltonian.

5.2 Velocity operator in presence of SOI interaction

It is usually admitted that the velocity operator $\widehat{\mathbf{v}}$ is equal to $\partial\widehat{\mathcal{H}}/\partial\widehat{\mathbf{p}}$ whatever the Hamiltonian $\widehat{\mathcal{H}}$. However, to the best of our knowledge, the derivation can be found only when $\widehat{\mathcal{H}}$ is quadratic in $\widehat{\mathbf{p}}$. Therefore a general derivation, in particular in the case of effective Hamiltonians, is mandatory. We start from Ehrenfest's theorem (valid whatever the Hamiltonian $\widehat{\mathcal{H}}$)

$$\langle\widehat{\mathbf{v}}\rangle = \frac{\mathrm{d}\langle\widehat{\mathbf{r}}\rangle}{\mathrm{d}t} = \frac{i}{\hbar}\left\langle \left[\widehat{\mathcal{H}},\, \widehat{\mathbf{r}}\right]\right\rangle \tag{5.7}$$

If $(i/\hbar)\left\langle \left[\widehat{\mathcal{H}},\, \widehat{\mathbf{r}}\right]\right\rangle = \left\langle \partial\widehat{\mathcal{H}}/\partial\mathbf{p}\right\rangle$, then $\widehat{\mathbf{v}} = \partial\widehat{\mathcal{H}}/\partial\widehat{\mathbf{p}}$ because two linear operators which have the same mean values over all possible states are equal: $\left\langle\widehat{A}\right\rangle = \left\langle\widehat{B}\right\rangle$ implies that $\widehat{A} = \widehat{B}$ [99, p. 633] Practically, it is enough to show that $(i/\hbar)\left[\widehat{\mathcal{H}},\, \widehat{\mathbf{r}}\right] = \partial\widehat{\mathcal{H}}/\partial\widehat{\mathbf{p}}$ to prove that $\widehat{\mathbf{v}} = \partial\widehat{\mathcal{H}}/\partial\widehat{\mathbf{p}}$.

First, considering the case $\widehat{\mathcal{H}} = \widehat{H}_0$ which contains a $\widehat{H}^{(2)}$ term (Eq. 3.1),

$(i/\hbar)\left[\widehat{H}_0,\,\widehat{\mathbf{r}}\right] = (\hbar/im)\,\widehat{\mathbf{p}} = \partial\widehat{H}_0/\partial\widehat{\mathbf{p}}$, for a system described by an Hamiltonian quadratic versus momentum components, and we obtain the velocity $\widehat{\mathbf{v}}_0$:

$$\widehat{\mathbf{v}}_0 = \frac{\partial\widehat{H}_0}{\partial\widehat{\mathbf{p}}}. \tag{5.8}$$

Second, we have to check that this relation still holds in the presence of SOI where the Hamiltonian is $\widehat{\mathcal{H}} = \widehat{H} = \widehat{H}_0 + \widehat{H}_{SO}$ (Eq. 3.3). In other words we want to show that

$$\widehat{\mathbf{v}} = \frac{\partial\widehat{H}}{\partial\widehat{\mathbf{p}}}. \tag{5.9}$$

We know that $\widehat{\mathbf{v}}_0 = (i/\hbar)\left[\widehat{H}_0,\,\widehat{\mathbf{r}}\right] = \partial\widehat{H}_0/\partial\widehat{\mathbf{p}}$. To show that Eq. 5.9 is valid, it is enough to show that $\widehat{\mathbf{v}}_{SO} = \partial\widehat{H}_{SO}/\partial\widehat{\mathbf{p}}$, which will give $\widehat{\mathbf{v}} = \partial\widehat{H}/\partial\widehat{\mathbf{p}}$ with $\widehat{\mathbf{v}} = \widehat{\mathbf{v}}_0 + \widehat{\mathbf{v}}_{SO}$. A straightforward calculation yields

$$\widehat{\mathbf{v}}_{SO} = \frac{i}{\hbar}[\widehat{H}_{SO},\,\widehat{\mathbf{r}}] = \frac{\hbar}{4m^2c^2}\left(\widehat{\sigma}\times\nabla\mathfrak{U}\right) = \frac{\partial\widehat{H}_{SO}}{\partial\widehat{\mathbf{p}}} \tag{5.10}$$

which proves Eq. 5.9: the derivative of the Hamiltonian, with respect to the momentum operator, still provides a suitable definition of the velocity when the SOI term is taken into account.

5.3 Velocity operator with an effective Hamiltonian $\widehat{H}_{eff}$

We generalize the results obtained in Sec. 5.2, to the case of a generic effective Hamiltonian $\widehat{\mathcal{H}} = \widehat{H}_{eff}$. Again we exploit Ehrenfest's theorem, as written in Eq. 5.7. Considering for instance the x component, we verify that

$$\left[\widehat{H}^{(n)},\,x\right] = \sum_{\alpha+\beta+\gamma=n} c^{\alpha\beta\gamma}\left(\frac{\hbar}{i}\right)\alpha\,\widehat{p}_x^{\alpha-1}\,\widehat{p}_y^{\beta}\,\widehat{p}_z^{\gamma} = \frac{\hbar}{i}\frac{\partial\widehat{H}^{(n)}}{\partial\widehat{p}_x} \tag{5.11}$$

or

$$\frac{i}{\hbar}\left[\widehat{H}_{\mathbf{p}},\,\widehat{\mathbf{r}}\right] = \frac{i}{\hbar}\left[\widehat{H}_{\mathbf{eff}},\,\widehat{\mathbf{r}}\right] = \frac{\partial\widehat{H}_{eff}}{\partial\widehat{\mathbf{p}}} \tag{5.12}$$

which proves that

$$\widehat{\mathbf{v}} = \frac{\partial \widehat{H}_{eff}}{\partial \widehat{\mathbf{p}}}. \quad (5.13)$$

Using Eqs. 5.3-5.6, it is then easy to calculate the j component $\widehat{v}_j^{(n)}$ $(j = x, y, z)$ of the velocity operator $\widehat{\mathbf{v}}^{(n)}$ associated to $\widehat{H}^{(n)}$:

$$\widehat{v}_j^{(n)} = \frac{\partial \widehat{H}^{(n)}}{\partial \widehat{p}_j} = nc_j\left(c_x\widehat{p}_x + c_y\widehat{p}_y + c_z\widehat{p}_z\right)^{n-1}. \quad (5.14)$$

We introduce the scalar product between the momentum $\widehat{\mathbf{p}}$ and the velocity operator $\widehat{\mathbf{v}}^{(n)}$

$$\widehat{p}_x\widehat{v}_x^{(n)} + \widehat{p}_y\widehat{v}_y^{(n)} + \widehat{p}_z\widehat{v}_z^{(n)} = n\left(c_x\widehat{p}_x + c_y\widehat{p}_y + c_z\widehat{p}_z\right)^n = n\widehat{H}^{(n)}. \quad (5.15)$$

With this notation, $\widehat{\mathbf{v}}_0$, introduced in the paragraph 5.2, is such that $\widehat{\mathbf{v}}_0 = \widehat{\mathbf{v}}^{(2)}$. Eq. 5.15 means that

$$\widehat{\mathbf{p}} \cdot \widehat{\mathbf{v}}^{(n)} = n\widehat{H}^{(n)} \quad (5.16)$$

and eventually

$$\widehat{H}_{eff}\psi = \left(\widehat{\mathbf{p}} \cdot \sum_n \frac{1}{n}\widehat{\mathbf{v}}^{(n)}\right)\psi + V\psi = E\psi. \quad (5.17)$$

As pointed out in Sec. 4, we are allowed to define current operators in open systems provided that we properly take into account their boundary conditions. We are interested in finding the form of the current operator $\widehat{\mathbf{J}} = \left(\widehat{J}_x, \widehat{J}_y, \widehat{J}_z\right)$ for an Hamiltonian $\widehat{H}^{(n)} + V(\mathbf{r})$ - the current operator being $\widehat{\mathbf{J}}^{(n)}$ - and more generally for the Hamiltonian $\widehat{H}_{eff} = \widehat{H}_{\mathbf{p}} + V(\mathbf{r}) = \sum_n \widehat{H}^{(n)} + V(\mathbf{r})$ (Eqs. 5.1-5.2) - the current operator being $\widehat{\mathbf{J}}$. For an Hamiltonian $\widehat{\mathbf{p}}^2/2m + V(\mathbf{r})$, it is known [99, p. 372] that the jth component of the current operator ($j = x,\ y,$ or z) at the point $\mathbf{r}_0$ is of the shape $\widehat{J}_j^{(2)}(\mathbf{r}_0) = (1/2m)\left[\delta_{\mathbf{r}_0}\widehat{p}_j + \widehat{p}_j\delta_{\mathbf{r}_0}\right]$, where $\delta_{\mathbf{r}_0}$ is the Dirac distribution, centered in $\mathbf{r} = \mathbf{r}_0$; with the notation of Eqs. 5.1-5.2, $\widehat{H}^{(2)} = \sum_{\substack{l(k)\in\{x,y,z\} \\ k=1,2}} c_{l(1),l(2)}\widehat{p}_{l(1)}\widehat{p}_{l(2)}$, $\widehat{J}_j^{(2)}(\mathbf{r}_0) = \sum_{l(1)=\{x,y,z\}} c_{j,l(1)}\left[\delta_{\mathbf{r}_0}\widehat{p}_{l(1)} + \widehat{p}_{l(1)}\delta_{\mathbf{r}_0}\right]$, $c_{l(1),l(2)} = (1/2m)\,\delta_{l(1),l(2)}$. The aim of the following procedure is to show that, for an Hamiltonian $H^{(n)} + V(\mathbf{r})$, the

following form of the jth component of the probability current operator

$$\hat{J}_j^{(n)}(\mathbf{r_0}) = \sum_{\substack{l(k)\in\{x,y,z\}\\ k=1,..,n-1}} c_{j,l(1),...,l(n-1)} \left[\delta_{\mathbf{r}_0}\widehat{p}_{l(1)}\widehat{p}_{l(2)}\cdots\widehat{p}_{l(n-1)} + \widehat{p}_{l(1)}\delta_{\mathbf{r}_0}\widehat{p}_{l(2)}\cdots\widehat{p}_{l(n-1)} + \ldots + \widehat{p}_{l(1)}\widehat{p}_{l(2)}\cdots\widehat{p}_{l(n-1)}\delta_{\mathbf{r}_0}\right] \quad (5.18)$$

gives back Eq. 4.11, where $\delta_{\mathbf{r}_0} = \delta(\mathbf{r}-\mathbf{r}_0)$ is again the Dirac distribution, which interacts with the mixed powers of the current operator so that the symmetrization procedure used in the construction of $\hat{J}_j^{(n)}(\mathbf{r_0})$ provides $(n-2)$ further summations with respect to $\widehat{J}_j^{(2)}(\mathbf{r}_0)$. The two definitions coincide only up to $n=2$. The extra terms are crucial in order to satisfy the continuity equation. We evaluate every term over a generic state ψ; for example the second term is of the shape

$$\begin{aligned}\left\langle\psi\left|\widehat{p}_{l(1)}\delta_{\mathbf{r}_0}\widehat{p}_{l(2)}\cdots\widehat{p}_{l(n-1)}\right|\psi\right\rangle &= \int \mathrm{d}^3r\ \psi^*\widehat{p}_{l(1)}\delta_{\mathbf{r}_0}\widehat{p}_{l(2)}\cdots\widehat{p}_{l(n-1)}\psi\\ &= \int \mathrm{d}^3r\ \left(\widehat{p}_{l(1)}\psi\right)^\dagger\delta_{\mathbf{r}_0}\widehat{p}_{l(2)}\cdots\widehat{p}_{l(n-1)}\psi\\ &= \left[\widehat{p}_{l(1)}\psi(\mathbf{r}_0)\right]^\dagger\widehat{p}_{l(2)}\cdots\widehat{p}_{l(n-1)}\psi(\mathbf{r}_0).\end{aligned} \quad (5.19)$$

Then the jth Cartesian component of probability current for a generic state $J_j[\psi]$ can be written as:

$$J_j^{(n)}[\psi] = \left\langle\psi\left|\hat{J}_j^{(n)}(\mathbf{r_0})\right|\psi\right\rangle = \sum_{\substack{l(k)\in\{x,y,z\}\\ k=1,..,n-1}} c_{j,l(1),...,l(n)}\left[\psi^\dagger\widehat{p}_{l(1)}\cdots\widehat{p}_{l(n-1)}\psi + \ldots + \left(\widehat{p}_{l(1)}\cdots\widehat{p}_{l(k-1)}\psi\right)^\dagger\widehat{p}_{l(k)}\cdots\widehat{p}_{l(n-1)}\psi + \ldots + \left(\widehat{p}_{l(1)}\cdots\widehat{p}_{l(n-1)}\psi\right)^\dagger\psi\right] \quad (5.20)$$

where $\psi = \psi(\mathbf{r}_0)$. From Eq. 5.20, we can find the generic divergence term related

to the derivative with respect to $\widehat{p}_j$:

$$\widehat{p}_j J_j^{(n)}[\psi] = \sum_{\substack{l(k)\in\{x,y,z\}\\ k=1,..n-1}} c_{j,l(1),...,l(n)} \Big[\psi^\dagger \widehat{p}_j \widehat{p}_{l(1)} \cdots \widehat{p}_{l(n-1)}\psi - \left(\widehat{p}_j\psi\right)^\dagger \widehat{p}_{l(1)} \cdots \widehat{p}_{l(n-1)}\psi$$
$$+ \left(\widehat{p}_{l(1)} \cdots \widehat{p}_{l(k-1)}\psi\right)^\dagger \widehat{p}_j \widehat{p}_{l(k)} \cdots \widehat{p}_{l(n-1)}\psi - \left(\widehat{p}_j \widehat{p}_{l(1)} \cdots \widehat{p}_{l(k-1)}\psi\right)^\dagger \widehat{p}_{l(k)} \cdots \widehat{p}_{l(n-1)}\psi$$
$$+ \left(\widehat{p}_{l(1)} \cdots \widehat{p}_{l(k)}\psi\right)^\dagger \widehat{p}_j \widehat{p}_{l(k+1)} \cdot\cdot \widehat{p}_{l(n-1)}\psi - \left(\widehat{p}_j \widehat{p}_{l(1)} \cdots \widehat{p}_{l(k)}\psi\right)^\dagger \widehat{p}_{l(k+1)} \cdots \widehat{p}_{l(n-1)}\psi$$
$$+ \ldots + \left(\widehat{p}_{l(1)} \cdots \widehat{p}_{l(n-1)}\psi\right)^\dagger \widehat{p}_j\psi - \left(\widehat{p}_j \widehat{p}_{l(1)} \cdots \widehat{p}_{l(n-1)}\psi\right)^\dagger \psi\Big]. \quad (5.21)$$

In Eq. 5.21 all the terms that have the same order in k (two consecutive terms but the first one and the last one) vanish after summation over j:

$$\sum_{j=\{x,y,z\}} \sum_{\substack{l(k)\in\{x,y,z\}\\ k=1,..n-1}} c_{j,l(1)}, \ldots, c_{l(n)} \Big[- \left(\widehat{p}_j \widehat{p}_{l(1)} \cdots \widehat{p}_{l(k-1)}\psi\right)^\dagger \widehat{p}_{l(k)} \cdots \widehat{p}_{l(n-1)}\psi$$
$$+ \left(\widehat{p}_{l(1)} \cdots \widehat{p}_{l(k)}\psi\right)^\dagger \widehat{p}_j \widehat{p}_{l(k+1)} \cdot\cdot \widehat{p}_{l(n-1)}\psi\Big] = 0 \quad (5.22)$$

Then the only terms still remaining in the summation are:

$$\sum_{j=\{x,y,z\}} \widehat{p}_j J_j^{(n)}[\psi] = \widehat{\mathbf{p}} \cdot \mathbf{J}^{(n)}[\psi]$$
$$= \sum_{j=\{x,y,z\}} \sum_{\substack{l(k)\in\{x,y,z\}\\ k=1,..,n-1}} c_{j,l(1)}, \ldots, c_{l(n)} \Big[\psi^\dagger \widehat{p}_j \widehat{p}_{l(1)} \cdots \widehat{p}_{l(n-1)}\psi - \left(\widehat{p}_j \widehat{p}_{l(1)} \cdots \widehat{p}_{l(n-1)}\psi\right)^\dagger \psi\Big]$$
$$= \sum_{j=\{x,y,z\}} \sum_{\substack{l(k)\in\{x,y,z\}\\ k=1,..,n-1}} 2i\, c_{j,l(1)}, \ldots, c_{l(n)} \mathrm{Im}\psi^\dagger \widehat{p}_j \widehat{p}_{l(1)} \cdots \widehat{p}_{l(n-1)}\psi. \quad (5.23)$$

Now $\nabla \cdot \mathbf{J}^{(n)}[\psi] = (i/\hbar)\widehat{\mathbf{p}} \cdot \mathbf{J}^{(n)}[\psi]$ and Eq. 5.24 results in a collection of pure imaginary terms and the final expression for the divergence of the probability current reads:

$$\nabla \cdot \mathbf{J}^{(n)}[\psi] = -\frac{2}{\hbar} \mathrm{Im} \sum_{j=\{x,y,z\}} \sum_{\substack{l(k)\in\{x,y,z\}\\ k=1,..,n-1}} c_{j,l(1),...,l(n)} \left(\psi \middle| \widehat{p}_j \widehat{p}_{l(1)} \cdots \widehat{p}_{l(n-1)} \middle| \psi\right). \quad (5.24)$$

Eventually

$$\nabla \cdot \mathbf{J}[\psi] = \sum_n \nabla \cdot \mathbf{J}^{(n)}[\psi].$$

Thus we have shown that the hermitian symmetrized probability-current operator of Eq. 5.18 satisfies the continuity equation for the effective Hamiltonian of Eq. 5.1.

Obviously, adding a term proportional to the curl of any vector field would not affect the result. Such a definition of $\hat{\mathbf{J}}$ provides an unambiguous and general tool for evaluating the probability current. Provided the Hamiltonian of the whole system is known, this probability-current operator guarantees the requirements of the continuity equation.

Now it is useful to introduce the Hermitian symmetrized velocity operator

$$\widehat{\mathfrak{v}}_j^{(n)}(\mathbf{r_0}) = \frac{n}{2} \sum_{\substack{l(k)\in\{x,y,z\} \\ k=1,..,n-1}} c_{j,l(1),\cdots,l(n-1)} \left[\delta_{\mathbf{r}_0} \widehat{p}_{l(1)} \cdots \widehat{p}_{l(n-1)} + \widehat{p}_{l(1)} \cdots \widehat{p}_{l(n-1)} \delta_{\mathbf{r}_0}\right] \quad (5.25)$$

For example for $n \geq 2$, the comparison between Eqs. 5.18 and 5.25 clearly shows that $\widehat{J}_j^{(n)}(\mathbf{r_0})$ contains $n-2$ extra terms, which are straightforwardly obtained from $\partial \widehat{H}_{eff}/\partial \widehat{\mathbf{p}}$. For instance, with $\widehat{H}_{eff} \equiv \widehat{p}^n$, we have $\partial \widehat{H}_{eff}/\partial \widehat{\mathbf{p}} \equiv n \widehat{p}^{n-1}$, so that:

$$\widehat{\mathfrak{v}}^{(n)}(\mathbf{r_0}) \equiv (n/2) \left(\delta_{\mathbf{r}_0} \widehat{p}^{n-1} + \widehat{p}^{n-1} \delta_{\mathbf{r}_0}\right), \quad (5.26)$$

whereas

$$\widehat{J}^{(n)}(\mathbf{r_0}) \equiv \left(\delta_{\mathbf{r}_0} \widehat{p}^{n-1} + \widehat{p} \delta_{\mathbf{r}_0} \widehat{p}^{n-2} + \ldots + \widehat{p}^{n-1} \delta_{\mathbf{r}_0}\right). \quad (5.27)$$

As shown in Ref. 83, extra terms are specially important for evanescent waves. Therefore, in the following we deal with tunneling problems.

5.4 BenDaniel-Duke-like formulation and boundary conditions

We stress that the central question when defining the current operators and related quantities is the proper definition of the system and of its boundaries. Dealing with heterojunctions, where each bulk medium is described by the relevant Hamiltonian, requires defining proper matching conditions at the

boundaries. In this sense, the BDD Hamiltonian [96] is the simplest smart approach that allows solution of the Schrödinger equation over the whole space while it guaranties the conservation of the probability current at the interface. The principle is the following. Let us consider a one-dimensional problem and two different media for $x < 0$ and $x > 0$. Each medium is characterized by its own Hamiltonian. The question is to find a solution of the Schrödinger equation, made of eigenfunctions of the relevant band of the two bulk materials, which ensures the continuity of the probability current at the origin. In this sense, the problem is analogous to a scattering problem, where the wave functions are determined only at some distance of the scattering potential. Proper matching conditions relevant to the extension of the bulk envelope functions at the origin will allow one to determine the envelope function over the whole space. For that, BBD propose writing an Hamiltonian over the whole space as $\widehat{p}_x [1/2m(x)] \widehat{p}_x + V(x)$ where $m(x)$ is the effective mass in each medium. The integration of this BDD Hamiltonian around the boundary automatically ensures the continuity of the probability current of Eq. 3.2, provided that $\psi(x)$ and $[1/m(x)][\partial\psi/\partial x]$ are continuous.

Now, consider two regions (1) and (2) and assume that each region is made of a given crystalline material. We look for the envelope function, solution of the Schrödinger equation, which is made from plane waves which are eigenstates of the crystal, inside each material. Observe that, near the interface, the crystal periodicity is broken so that the true Hamiltonian and the true eigenfunctions will become involved. The principle is then to define proper matching conditions applying to the prolongation of the envelope function at the origin. For that purpose, we consider a volume $\mathbb{V}$, limited by a surface $\mathbb{S}$, that surrounds an interface portion. Similarly to the BDD technique, we start from Eq. 5.17 and we integrate the Schrödinger equation over $\mathbb{V}$. Using Ostrogradski's theorem, when $\mathbb{V}$ tends to zero, we obtain

$$\lim_{\mathbb{V} \longrightarrow 0} \int_{\mathbb{S}} \left(\sum_n \frac{1}{n} \mathbf{v}^{(n)} \psi \right) \cdot \mathrm{d}\mathbf{s} = 0 \tag{5.28}$$

where d$\mathbf{s}$ is normal to the surface $\mathbb{S}$.

For a one dimensional case with the interface at the origin, Eq. 5.28 becomes:

$$\lim_{\varepsilon\to 0}\left[\sum_n \frac{1}{n} v^{(n)}\psi\right]_{-\varepsilon}^{+\varepsilon} = 0 \tag{5.29}$$

Let us again emphasize that no information is obtained on the true wave function near the origin. Eq. 5.29 does not ensure either the continuity of the envelope function or the existence of derivatives *at* the interface.

As an illustration, let us consider the case of a Rashba Hamiltonian

$$\hat{H}_{eff} = a\widehat{p} + b\widehat{p}^2 \tag{5.30}$$

where a and b are two Hermitian matrices. According to Eq. 5.29, we can write down the first continuity condition as follows:

$$[a\psi + b\widehat{p}\psi]_{-\varepsilon}^{+\varepsilon} = 0. \tag{5.31}$$

Using this condition to solve the problem, and adding *a priori* the continuity of the envelope function at the interface as a second condition, we verify that the probability current is indeed continuous at the interface:

$$J[\psi] = \langle \psi \mid a + b\widehat{p} \mid \psi \rangle + c.c. \tag{5.32}$$

Then, the jump of the derivative of the wave function at the interface is determined by

$$[b\widehat{p}\psi]_{-\varepsilon}^{+\varepsilon} = -\,[a]_{-\varepsilon}^{+\varepsilon}\psi(0). \tag{5.33}$$

It is clear then that the BDD approach, introduced to solve a problem with a quadratic Hamiltonian, is also suitable to obtain a solution when a Rashba contribution is added; then we can say that up to the second order in the momentum-power series expansion of the Hamiltonian, the continuity of a "generalized velocity" (see Eq. 5.29) and the continuity of the wave function at the interface imply the conservation of the probability current at this point. Remarkably, the boundary conditions that we need to solve the problem drastically change when moving to the case of a DP Hamiltonian with cubic terms. The

crucial point, that we address in the following, is that we cannot make any hypothesis about the continuity of the wave function because, if we need to ensure probability-current conservation at an interface, we must accept an envelope function ψ which is no longer continuous.

To give an insight into the expression of the current operator and into the conservation of the probability current, let us again come back to an interface between two semi-infinite one-dimensional media (1) and (2). In each bulk crystal, the relevant Hamiltonian is

$$\widehat{H}_r = \sum_n \widehat{H}_r^{(n)} + V_r \tag{5.34}$$

with

$$\widehat{H}_r^{(n)} = \gamma_r^{(n)} \widehat{p}^n \tag{5.35}$$

with $r = 1$ or $r = 2$ depending on wether $x < 0$ or $x > 0$. $\widehat{H}_r$ admits the eigenfunctions φ_r, associated to the fixed energy E which verify

$$\widehat{H}_r \varphi_r = E \varphi_r. \tag{5.36}$$

We consider the Hamiltonian extended over the whole space as

$$\widehat{\mathfrak{H}} = \Theta(-x)\widehat{H}_1 + \Theta(x)\widehat{H}_2 \tag{5.37}$$

where $\Theta(x)$ is the Heaviside function.

However, strictly speaking, near the heterojunction the spatial periodicity is broken, so that over a few Wigner-Seitz cells, the true Hamiltonian differs (it possibly includes interface terms) and the electron states are no longer pure Bloch states. We consider two coordinates, $-w_1$ and w_2, so that, in the bulk regions $]-\infty, -w_1]$ and $[w_2, +\infty[$ the electronic structure remains unaffected. Very close to the heterojunction, the eigenfunctions are not assumed to be explicitly known. We consider a wave function ψ which is an eigenstate of the Hamiltonian over the whole space at energy E. We expect that, over the domain $]-\infty, -w_1] \cup [w_2, +\infty[$, ψ coincides with $\Psi = \Theta(-x - w_1)\varphi_1 + \Theta(x - w_2)\varphi_2$ (we assume that

the matching is sufficiently regular). Thus, we have

$$\left\langle \Psi \middle| \widehat{\mathfrak{H}} \middle| \psi \right\rangle = E \left[\langle \varphi_1 \mid \varphi_1 \rangle_{(1)} + \langle \varphi_2 \mid \varphi_2 \rangle_{(2)} \right] \tag{5.38}$$

where $\langle | \rangle_{(r)}$ means summation over the bulk part of region (r). Because the total probability in the domain $]-\infty, -w_1] \cup [w_2, +\infty[$ has to be conserved, from Ehrenfest's theorem [Eq. 4.8 with $\widehat{A} = \Theta(-x - w_1) + \Theta(x - w_2)$] we must have

$$\langle \psi | [\Theta(-x - w_1) + \Theta(x - w_2), \mathfrak{H}] | \psi \rangle = \left\langle \psi \middle| \widehat{\mathfrak{H}} \middle| \Psi \right\rangle - \left\langle \Psi \middle| \widehat{\mathfrak{H}} \middle| \psi \right\rangle = 0, \tag{5.39}$$

i. e.,

$$\left\langle \Psi \middle| \widehat{\mathfrak{H}} \middle| \psi \right\rangle = \left\langle \psi \middle| \widehat{\mathfrak{H}} \middle| \Psi \right\rangle = E \langle \psi \mid \Psi \rangle . \tag{5.40}$$

Observe that:

$$\begin{aligned} \widehat{H}_1^{(n)} [\Theta(-x - w_1) \varphi_1] &= \gamma_1^{(n)} \widehat{p}^n \Theta(-x - w_1) \varphi_1 \\ &= \Theta(-x - w_1) \gamma_1^{(n)} \widehat{p}^n \varphi_1 \\ &+ i\hbar \gamma_1^{(n)} \left[\delta(x + w_1) \widehat{p}^{n-1} + \widehat{p} \delta(x + w_1) \widehat{p}^{n-2} + \right. \\ &\left. + \ldots + \widehat{p}^{n-1} \delta(x + w_1) \right] \varphi_1 \\ &= \Theta(-x - w_1) \gamma_1^{(n)} \widehat{p}^n \varphi_1 + i\hbar \widehat{J}_1^{(n)} (-w_1) \varphi_1 \end{aligned} \tag{5.41}$$

So that

$$\widehat{H}_1 [\Theta(-x - w_1) \varphi_1] = E \Theta(-x - w_1) \varphi_1 + i\hbar \widehat{J}_1 (-w_1) \varphi_1 \tag{5.42}$$

and similarly

$$\widehat{H}_2 [\Theta(x + w_2) \varphi_2] = E \Theta(x - w_2) \varphi_2 - i\hbar \widehat{J}_2 (w_2) \varphi_2 . \tag{5.43}$$

Eventually

$$\widehat{\mathfrak{H}} \Psi = E \Psi + i\hbar \left[\widehat{J}_1 (-w_1) \varphi_1 - \widehat{J}_2 (w_2) \varphi_2 \right] \tag{5.44}$$

Then, Eq. 5.40 is satisfied provided that

$$\widehat{J}_2 [\varphi_2 (w_2)] = \widehat{J}_1 [\varphi_1 (-w_1)] . \tag{5.45}$$

The important point is not the conservation relation, which might appear as physically obvious, but that, in Eqs. 5.41 and 5.43, the symmetrized current operator is automatically generated in the form derived in Eq. 5.18, providing a physical insight into this mathematical expression. Because we only deal with wave functions at some distance from the heterojunction, the continuity of the true wave function at $x = 0$ does not implies the continuity of the envelope function Ψ which may be discontinuous. This is in line with the considerations of Harrison [97]. Eq. 5.29 and 5.45 generate a set of boundary conditions relevant to the tunneling problem.

5.5 The [110]-oriented GaAs barrier

We analyze the case of electron tunneling under normal incidence through a [110]-oriented GaAs barrier, which was shown to be non trivial and solved in special cases in Ref. 83. The importance of this particular tunneling configuration can be well explained by the following argument: if we consider the Γ_{6c} conduction band of a non-centrosymmetric III-V semiconductor compound, like GaAs, in the small $\mathbf{k}$ approximation, we can give an analytical expression of the level splitting due to the Dresselhaus term [100], which has a k^3 dependence versus wave-vector:

$$E_{\pm} = \frac{\hbar}{2m^*}\left(k_x^2+k_y^2+k_z^2\right)+\gamma\sqrt{k_x^2\left(k_y^2-k_z^2\right)^2+k_y^2\left(k_z^2-k_x^2\right)^2+k_z^2\left(k_x^2-k_y^2\right)^2} \tag{5.46}$$

where γ is the strength of the effective D'yakonov-Perel magnetic field [77, 78], which removes the spin degeneracy. Indeed it is straightforward to see that along the [110]-direction the spin-splitting is maximum so that this crystallographic axes is really useful to study the effects of SOI term in GaAs. Concerning with tunneling heterojunctions, we are interested in evanescent waves in the [110]-oriented GaAs barrier. At this purpose, looking at the Hamiltonian of Eq. 5.46, it is possible to see that the k^3-dependence of the DP field does not allow pure imaginary tunneling wave-vector so that, in order to deal with real energy lines, we have to take into account the complex wave vector $\mathbf{k} = \frac{1}{\sqrt{2}}(Q \pm iK)[110]$ [83]. For complete treatment of evanescent states in non-centrosymmetric III-V

semiconductors, the reader is invited to refer to Ref. 101.

Hereafter, we apply the tools and boundary conditions presented in this paper to solve it in a more simple and general manner. We confirm and generalize the results derived in Ref. 83. In particular, we are able to solve the problem of an heterojunction between a free-electron media and a semiconductor without inversion center, where the DP field is a step function, which remained puzzling. In the $[110]$ direction, the one dimensional DP Hamiltonian is:

$$\widehat{H}_{DP} = \frac{\gamma_c}{\hbar^2}\widehat{p}^2 \pm \frac{\gamma}{2\hbar^3}\widehat{p}^3 \tag{5.47}$$

where $+$ $(-)$ refers to the up (down)- spin channel quantized along the DP field direction. We consider as solution a general wavefunction written as follows:

$$\psi = \alpha\left(\psi_0 + \frac{i\beta}{\hbar\gamma_c k^2}\gamma_c\widehat{p}\psi_0\right)e^{i\chi z} \tag{5.48}$$

where ψ_0 is the zeroth order function that is a solution of the tunneling problem with energy E and with the potential V when SOI is turned off. Here $\gamma_c k^2 = E - V$, α and β are complex parameters to be determined, and χ is a real (see below) wavevector component which is added to k when SOI is turned on. We have the relations

$$\widehat{p}\psi = \alpha\left(\widehat{p}\psi_0 + i\frac{\beta}{\hbar\gamma_c k^2}\gamma_c\,\widehat{p}^2\,\psi_0\right)e^{i\chi z} + \hbar\chi\psi, \tag{5.49}$$

$$\widehat{p}^2\psi = \hbar^2\left(\frac{E-V}{\gamma_c} - \chi^2\right)\psi + 2\hbar\chi\widehat{p}\psi. \tag{5.50}$$

We calculate the velocity operators from Eq. 5.14

$$\frac{1}{2}v^{(2)} + \frac{1}{3}v^{(3)} = \frac{\gamma_c}{\hbar^2}\widehat{p} \pm \frac{\gamma}{2\hbar^3}\widehat{p}^2 \tag{5.51}$$

and, according to Eq. 5.29, we find the matching condition

$$\left[\gamma_c\left(1 \pm \frac{\gamma}{\gamma_c}\chi\right)\widehat{p}\psi\right]_{-\varepsilon}^{+\varepsilon} = \mp\left[\frac{1}{2}\gamma\hbar\left(\frac{E-V}{\gamma_c} - \chi^2\right)\psi\right]_{-\varepsilon}^{+\varepsilon} \tag{5.52}$$

which is a generalization of Eq. (3.50) of Ref. 83.

Now, we have to satisfy the conservation of the probability current

$$J[\psi] = \frac{\gamma_c}{\hbar^2}\left(1 \pm \frac{\gamma}{\gamma_c}\chi\right)\left[\psi^* \widehat{p}\psi + \psi\left(\widehat{p}\psi\right)^*\right] \pm \frac{\gamma}{\hbar}\left(\frac{E-V}{\gamma_c} - \chi^2\right)|\psi|^2 \pm \frac{\gamma}{2\hbar^3}\left|\widehat{p}\psi\right|^2. \tag{5.53}$$

We obtain here an important result: *The envelope function cannot be continuous at the interface.* Indeed, assume ψ to be continuous. Then, after Eq. 5.52, we see that the last term in Eq. 5.53, that we rewrite as $\pm\left(1/2\hbar^3\right)\left(\gamma/\gamma_c^2\right)\gamma_c^2\left|\widehat{p}\psi\right|^2$ must be continuous. This is not possible since $\gamma_c \widehat{p}\psi_0$ is continuous (unless γ/γ_c^2 is almost continuous, which would be fortuitous).

We have to determine ψ complying the boundary conditions, which is not simple because the expression providing the current is not a linear function of ψ. However, if we consider γ as a first-order quantity and look for a solution to first order only, the result is surprisingly simple, as shown below. From the Schrödinger equation - Eq. 5.47 -, we find that χ verifies

$$\gamma_c\left(2k\chi + \chi^2\right) \pm \frac{\gamma}{2}\left(k^3 + 3k^2\chi + 3k\chi^2 + \chi^3\right) = 0 \tag{5.54}$$

then

$$\chi \simeq \mp\frac{1}{4}\frac{\gamma}{\gamma_c}k^2 = \mp\frac{1}{4}\frac{\gamma}{\gamma_c}\frac{E-V}{\gamma_c}. \tag{5.55}$$

As stated above, χ is a *real* quantity. For each spin, there are two others roots of the cubic equation (Eq. 5.54) which are much larger than the width of the Brillouin zone ; These two roots are of the order of γ_c/γ which is about 2 Å (two times the Brillouin zone width) in GaAs (see Fig. 4 of Ref. 83) and have no physical meaning. Note that, the cubic DP term, obtained from perturbation expansion, only holds for small wave vectors, a few percent of the Brillouin zone, so that taking into account these two other roots would be meaningless. From Eq. 5.48, we see that, upon tunneling, the up- and down- spin electrons undergo opposite phase shifts, which is equivalent to a precession around the DP-field direction. This would be quite intuitive if the field were not a complex quantity, and constitutes a prediction which can be experimentally tested. Let us calculate

the current at the interface ($z = z_0$) to first order

$$J[\psi(z_0)] = |\alpha|^2 \frac{\gamma_c}{\hbar^2} \left[\psi_0^* \widehat{p}\psi_0 + \psi_0 \left(\widehat{p}\psi_0\right)^*\right] + \frac{\gamma_c}{2\hbar}\left[2|\alpha|^2(\chi - \mathrm{Im}\beta) \pm \frac{\gamma}{\gamma_c}\frac{E-V}{\gamma_c}\right]|\psi_0|^2 + \frac{\gamma_c}{\hbar^3}\left[-|\alpha|^2\frac{2\gamma_c}{E-V}\mathrm{Im}\beta \mp \frac{\gamma}{2\gamma_c}\right]|\widehat{p}\psi_0|^2 \tag{5.56}$$

where the values of ψ_0 and of its derivative are taken at $z = z_0$. Observe that with the choice

$$|\alpha|^2 = 1 \quad \text{and} \quad \mathrm{Im}\beta = -\chi \tag{5.57}$$

the second and the last terms of Eq. 5.56 vanish so that

$$J[\psi(z_0)] = \frac{\gamma_c}{\hbar^2}\left[\psi_0^* \widehat{p}\psi_0 + \psi_0 \left(\widehat{p}\psi_0\right)^*\right] = J^f[\psi(z_0)] \tag{5.58}$$

where $J^f[\psi(z_0)]$ results from the application of the free-electron current operator. Thus, we obtain another essential result: *To first order, turning on the SOI does not alter the value of the probability current.* Consequently, to solve the problem we have only to show that ψ, given by Eq. 5.48 and with the conditions defined in Eq. 5.57, can match the boundary condition expressed by Eq. 5.52. We obtain

$$\alpha e^{i\chi z_0}\left(\gamma_c\widehat{p} + i\hbar\gamma_c \mathrm{Re}\beta\right)\psi_0 \quad \text{continuous.} \tag{5.59}$$

The continuity of Eq. 5.59 can always be ensured by taking $\alpha e^{i\chi z_0}$ continuous and $\mathrm{Re}\beta = 0$. Observe that the continuity of $\alpha e^{i\chi z_0}$ propagates a phase shift throughout the heterostructure.For instance, the first interface being taken at $z_0 = 0$, we can chose $\alpha = 1$ for the incident/reflected wave and for the evanescent wave in the barrier, whereas for the transmitted wave $\alpha = e^{i\chi\ell}$, where ℓ is the barrier thickness. Finally, we calculate ψ according to Eq. 5.48

$$\psi = \alpha e^{i\chi z}\left(\psi_0 \mp \frac{1}{4\hbar}\frac{\gamma}{\gamma_c^2}\gamma_c\widehat{p}\psi_0\right) \tag{5.60}$$

and we deduce the jump of ψ at the interface

$$[\psi(0)]_{z_{0-}}^{z_{0+}} = \left[\frac{\chi}{\hbar(E-V)}\right]_{z_{0-}}^{z_{0+}} (\gamma_c \widehat{p}\psi_0) = \mp\frac{1}{4\hbar}\left[\frac{\gamma}{\gamma_c^2}\right]_{z_{0-}}^{z_{0+}} (\gamma_c \widehat{p}\psi_0). \tag{5.61}$$

When γ/γ_c^2 is a constant, ψ is continuous and we recover the result derived by another technique in Ref. 83 (constant mass and constant γ).

Eq. 5.60 constitutes an important practical tool, which allows one to deduce the envelope function for conduction states in any [110]-oriented III-V semiconductors heterojunction when SOI is taken into account from the envelope function calculated when SOI is neglected.

5.6 Spin Current

So far, we have considered the definition of a novel probability-current operator, which can be widely used whatever the degree of the effective hamiltonian is and which induces new boundary conditions for tunneling heterostructure. As explained above, the key point of the subject relies on the good symmetrization of the velocity operator: in this section, we will see that the same argument can be applied also when considering the spin-current, which is the second fundamental quantity to analyzed in transport phenomena in presence of SOI.

The commonly accepted definition of the (6×6) spin current tensor is the symmetrized dyadic product:

$$\widehat{J}^{\uparrow\downarrow} = \frac{1}{2}\left(\widehat{\mathbf{v}}\widehat{\sigma}^t + \widehat{\sigma}\widehat{\mathbf{v}}^t\right) \tag{5.62}$$

where $\widehat{\sigma}$ is the spin operator and the velocity operator is $\partial\widehat{H}/\partial\mathbf{p}$ as usual,with the relevant Hamiltonian of the system $\widehat{H}$. The difficulties of such a definition can be appreciated through the continuity equation of Eq. 4.1: in fact the source term G is not properly defined (this problem is not relvant for particle current due to the fact that $G=0$, as explained in Sec. 4) in the sense that it can be modified and partially introduced in the expression of the current divergence, so that only $\mathbf{J}$ and G together have physical meaning [91]. Concerning with spintronics, the

source term is generally related to “spin-transfer torque ”. Then it is clear that the problem of defining both the spin current and source term can lead to ambiguous situations, ezpecially when the boundary conditions of the system are not properly specified.

At this purpose, we have shown in Sec. 5.5 that Eq. 5.18 provides a general and symmetrized definition of the probability-current operator. Following the conceptual scheme developed in Ref. 91, we can define the spin currents in the up- and down-spin channels by taking $\widehat{A} = \widehat{\pi}_s$, where $\widehat{\pi}_s$ is the orthogonal projector on the spin basis ($s = \pm$). Then the SC current $\delta\mathbf{J}_{\mathbf{u},j}[\psi]$, that arises from the difference between the up-spin and the down-spin current, is obtained by taking $\widehat{A} = \widehat{\sigma}_{\mathbf{u}}$, the Pauli operator along the **u** direction defining the quantization axis. It is straightforward to see that, as in Ref. 91, the j-component of the spin-current operator is obtained from the j-component of the probability-current operator after the substitution

$$c'_{j,l(1),\ldots,l(n)} = \frac{1}{2}\{\sigma_{\mathbf{u}}, c_{j,l(1),\ldots,l(n)}\}. \tag{5.63}$$

Because the spin current may be not conserved, there exist source terms

$$G = \frac{1}{\hbar}\mathrm{Im}\left(\psi^\dagger\left[\widehat{\sigma}_{\mathbf{u}}, \widehat{\mathcal{H}}\right]\psi\right). \tag{5.64}$$

BIBLIOGRAPHY

[1] Zutić, I., Fabian, J., and Das Sarma, S. *Reviews of Modern Physics* **76**(2), 323–410 April (2004).

[2] Meier, F. and Zakharchenya, B. P., editors. *Optical orientation (Modern Problems in Condensed Matter Sciences, Vol. 8)*. Elsevier, Amsterdam, (1984).

[3] Spicer, W. E. *Applied Physics* **12**(2), 115–130 February (1977).

[4] Pierce, D. and Meier, F. *Physical Review B* **13**(12), 5484–5500 June (1976).

[5] Pierce, D. and Meier, F. *Physical Review B* **13**(12), 5484–5500 June (1976).

[6] Miller, R., Kleinman, D., Nordland, W., and Gossard, A. *Physical Review B* **22**(2), 863–871 July (1980).

[7] Alvarado, S. F. *Applied Physics Letters* **39**(8), 615 (1981).

[8] Ciccacci, F., Drouhin, H.-J., Hermann, C., Houdré, R., and Lampel, G. *Applied Physics Letters* **54**(7), 632 (1989).

[9] Ciccacci, F., Molinari, E., and Christensen, N. E. *Solid State Communications* **62**(1), 1–3 April (1987).

[10] Ciccacci, F., Drouhin, H.-J., Hermann, C., Houdré, R., Lampel, G., and Alexandre, F. *Solid State Electronics* **31**(3-4), 489–492 (1988).

[11] Nakanishi, T. *Physics Letters A* **158**(6-7), 345–349 September (1991).

[12] Maruyama, T., Garwin, E., Prepost, R., Zapalac, G., Smith, J., and Walker, J. *Physical Review Letters* **66**(18), 2376–2379 May (1991).

[13] Mamaev, Y. A., Gerchikov, L. G., Yashin, Y. P., Vasiliev, D. A., Kuzmichev, V. V., Ustinov, V. M., Zhukov, A. E., Mikhrin, V. S., and Vasiliev, A. P. *Applied Physics Letters* **93**(8), 081114 (2008).

[14] Ciccacci, F., De Rossi, S., Pelucchi, E., and Tagliaferri, A. *Review of Scientific Instruments* **68**(4), 1841 (1997).

[15] Clendenin, J., Brachmann, A., Garwin, E., Harvey, S., Jiang, J., Kirby, R., Luh, D., Maruyama, T., Prepost, R., and Prescott, C. *Nuclear Instruments and Methods in Physics Research Section A: Accelerators, Spectrometers, Detectors and Associated Equipment* **536**(3), 308–311 January (2005).

[16] Pfalz, S., Winkler, R., Nowitzki, T., Reuter, D., Wieck, A., Hägele, D., and Oestreich, M. *Physical Review B* **71**(16), 1–11 April (2005).

[17] Lau, W. H., Sih, V., Stern, N. P., Myers, R. C., Buell, D. A., Gossard, A. C., and Awschalom, D. D. *Applied Physics Letters* **89**(14), 142104 (2006).

[18] Kosaka, H., Shigyou, H., Mitsumori, Y., Rikitake, Y., Imamura, H., Kutsuwa, T., Arai, K., and Edamatsu, K. *Physical Review Letters* **100**(9), 1–4 March (2008).

[19] Lampel, G. *Physical Review Letters* **20**(10), 491–493 March (1968).

[20] Allenspach, R., Meier, F., and Pescia, D. *Physical Review Letters* **51**(23), 2148–2150 December (1983).

[21] Allenspach, R., Meier, F., and Pescia, D. *Applied Physics Letters* **44**(12), 1107 (1984).

[22] Virgilio, M. and Grosso, G. *Physical Review B* **80**(20), 1–8 November (2009).

[23] Li, P. and Dery, H. *Physical Review Letters* **105**(3), 3–6 July (2010).

[24] Rioux, J. and Sipe, J. E. *Physical Review B* **81**(15), 27–30 April (2010).

[25] Grenet, L., Jamet, M., Noé, P., Calvo, V., Hartmann, J.-M., Nistor, L. E., Rodmacq, B., Auffret, S., Warin, P., and Samson, Y. *Applied Physics Letters* **94**(3), 032502 (2009).

[26] Loren, E. J., Ruzicka, B. A., Werake, L. K., Zhao, H., van Driel, H. M., and Smirl, A. L. *Applied Physics Letters* **95**(9), 092107 (2009).

[27] Shuto, Y., Tanaka, M., and Sugahara, S. *Journal of Applied Physics* **99**(8), 08D516 (2006).

[28] Bonfanti, M., Grilli, E., Guzzi, M., Virgilio, M., Grosso, G., Chrastina, D., Isella, G., von Känel, H., and Neels, A. *Physical Review B* **78**(4), 4–7 July (2008).

[29] Chaisakul, P., Marris-Morini, D., Isella, G., Chrastina, D., Izard, N., Le Roux, X., Edmond, S., Coudevylle, J.-R., and Vivien, L. *Applied Physics Letters* **99**(14), 141106 (2011).

[30] Isella, G. *Solid-State Electronics* **48**(8), 1317–1323 August (2004).

[31] Bassani, F. and Pastori Parravicini, G. *Electronic states and Optical Transitions in Solids*. Pergamon Press, Oxford, (1975).

[32] Wigner, E. P. *Group Theory and Its Application to the Quantum Mechanics of Atomic Spectra*. Academic Press Inc., New York, (1959).

[33] Koster, G. *Physical Review* **109**(2), 227–231 January (1958).

[34] Allenspach, R. and Pescia, D. *Physical Review B* **29**(4), 1783–1790 February (1984).

[35] Yu, P. Y. and Cardona, M. *Fundamentals of Semiconductors*. Springer, 3st edition, (2001).

[36] Koster, G. F., Dimmock, J. O., Wheeler, R. G., and Statz, H. *The Properties of the Thirty-Two Point Groups*. MIT Press Cambridge (Mass.), (1963).

[37] Cardona, M. and Pollak, F. *Physical Review* **142**(2), 530–543 February (1966).

[38] Tinkham, M. *Group Theory and Quantum Mechanics*. McGraw-Hill Inc., (1964).

[39] Goldstein, B. *Journal of Applied Physics* **44**(9), 4244 (1973).

[40] Rössner, B., Chrastina, D., Isella, G., and von Känel, H. *Applied Physics Letters* **84**(16), 3058 (2004).

[41] Ma, Q., Wang, K., and Schulman, J. *Physical Review B* **47**(4), 1936–1953 January (1993).

[42] People, R. *Physical Review B* **32**(2), 1405–1408 July (1985).

[43] Bir, G. L. and Pikus, G. E. *Symmetry & Strain-Induced effects in Semiconductors*. John Wiley and Sons Inc., New York, (1974).

[44] Fishman, G. *Semi-conducteurs: les bases de la théorie k.p*. Ecole Polytechnique, (2010).

[45] Bahder, T. *Physical Review B* **41**(17), 11992–12001 June (1990).

[46] Gell, M. *Physical Review B* **41**(11), 7611–7614 April (1990).

[47] Enders, P., Bärwolff, A., Woerner, M., and Suisky, D. *Physical Review B* **51**(23), 16695–16704 June (1995).

[48] Rideau, D., Feraille, M., Ciampolini, L., Minondo, M., Tavernier, C., Jaouen, H., and Ghetti, A. *Physical Review B* **74**(19), 1–20 November (2006).

[49] Matthews, J. W. *Journal of Applied Physics* **41**(9), 3800 (1970).

[50] Dismukes, J. P., Ekstrom, L., and Paff, R. J. *Journal of Physical Chemistry* **68**(10), 3021–3027 October (1964).

[51] Wortman, J. J. and Evans, R. A. *Journal of Applied Physics* **36**(1), 153 (1965).

[52] Ciccacci, F., De Rossi, S., and Campbell, D. M. *Review of Scientific Instruments* **66**(8), 4161 (1995).

[53] Bottegoni, F., Isella, G., Cecchi, S., and Ciccacci, F. *Applied Physics Letters* **98**(24), 242107 (2011).

[54] Ciccacci, F., Vescovo, E., Chiaia, G., De Rossi, S., and Tosca, M. *Review of Scientific Instruments* **63**(6), 3333 (1992).

[55] Gay, T. J. and Dunning, F. B. *Review of Scientific Instruments* **63**(2), 1635 (1992).

[56] Dimoulas, a., Tsipas, P., Sotiropoulos, A., and Evangelou, E. K. *Applied Physics Letters* **89**(25), 252110 (2006).

[57] Houdré, R., Hermann, C., Lampel, G., Frijlink, P., and Gossard, A. *Physical Review Letters* **55**(7), 734–737 August (1985).

[58] Klimeck, G., Oyafuso, F., Boykin, T. B., Bowen, R. C., and Allmen, P. V. *Computer Modeling in Engineering & Sciences* **3**(5), 601–642 (2002).

[59] Pierce, D. T., Celotta, R. J., Wang, G.-C., Unertl, W. N., Galejs, A., Kuyatt, C. E., and Mielczarek, S. R. *Review of Scientific Instruments* **51**(4), 478 (1980).

[60] Isella, G., Bottegoni, F., Pezzoli, F., Cecchi, S., Gatti, E., Chrastina, D., Grilli, E., Guzzi, M., and Ciccacci, F. In *SPIE Proceedings vol. 8100*, volume 4, 810007–810007–7, (2011).

[61] Ishikawa, Y., Wada, K., Liu, J., Cannon, D. D., Luan, H.-C., Michel, J., and Kimerling, L. C. *Journal of Applied Physics* **98**(1), 013501 (2005).

[62] Eisberg, R. and Resnik, R. *Quantum Physics of Atoms, Molecules, Solids, Nuclei, and Particles*. John Wiley and Sons Inc., New York, (1985).

[63] Davies, J. H. *The Physics of Low Dimensional Semiconductors: an introduction*. Cambridge University Press, (1998).

[64] Hanson, R. and Awschalom, D. D. *Nature* **453**(7198), 1043–9 June (2008).

[65] Dash, S. P., Sharma, S., Patel, R. S., de Jong, M. P., and Jansen, R. *Nature* **462**(7272), 491–4 November (2009).

[66] Jonker, B. T., Kioseoglou, G., Hanbicki, A. T., Li, C. H., and Thompson, P. E. *Nature Physics* **3**(8), 542–546 July (2007).

[67] Appelbaum, I., Huang, B., and Monsma, D. J. *Nature* **447**(7142), 295–8 May (2007).

[68] Jansen, R., Min, B.-C., and Dash, S. P. *Nature materials* **9**(2), 133–8 February (2010).

[69] Parsons, R. *Physical Review Letters* **23**(20), 1152–1154 November (1969).

[70] Luttinger, J. *Physical Review* **102**(4), 1030–1041 May (1956).

[71] Zhou, X., van Driel, H., and Mak, G. *Physical Review B* **50**(8), 5226–5230 August (1994).

[72] `http://www.wsi.tu-muenchen.de/nextnano3/`.

[73] Lange, C., Köster, N., Chatterjee, S., Sigg, H., Chrastina, D., Isella, G., von Känel, H., Schäfer, M., Kira, M., and Koch, S. *Physical Review B* **79**(20), 1–4 May (2009).

[74] Claussen, S. A., Tasyurek, E., Roth, J. E., and Miller, D. A. B. *Optics Express* **18**(25), 25596 November (2010).

[75] Zhang, P. and Wu, M. *Physical Review B* **80**(15), 1–11 October (2009).

[76] Bottegoni, F., Drouhin, H.-J., Fishman, G., and Wegrowe, J.-E. *ArXiv* **1109.5097v**, 23 September (2011).

[77] D'yakonov, M. and Perel, V. I. *Zh. Eksp. Teor. Fiz.* **60**, 1954 (1971).

[78] D'yakonov, M. and Perel, V. I. *Sov. Phys. JETP* **33**, 1053 (1971).

[79] Rashba, E. I. and Sheka, V. I. *Landau Level Spectroscopy, edited by G. Landwher and E. I. Rashba*. Elsevier, Amsterdam, (1991).

[80] Rashba, E. and Efros, A. *Physical Review Letters* **91**(12), 2–5 September (2003).

[81] Efros, A. and Rashba, E. *Physical Review B* **73**(16), 1–20 April (2006).

[82] Cohen-Tannoudji, C., Diu, B., and Laloë, F. *Mecanique Quantique*. Hermann, Paris, (1996).

[83] Nguyen, T., Drouhin, H.-J., Wegrowe, J.-E., and Fishman, G. *Physical Review B* **79**(16) April (2009).

[84] Rashba, E. *Physical Review B* **70**(20), 1–4 November (2004).

[85] Rashba, E. *Physical Review B* **68**(24), 5–7 December (2003).

[86] Sinova, J., Culcer, D., Niu, Q., Sinitsyn, N., Jungwirth, T., and MacDonald, A. *Physical Review Letters* **92**(12), 1–4 March (2004).

[87] Sonin, E. *Physical Review B* **76**(3), 1–4 July (2007).

[88] Sonin, E. *Physical Review B* **77**(3), 39901–39901 January (2008).

[89] Sonin, E. *Physical Review B* **82**(11), 1–4 September (2010).

[90] Li, Y. and Tao, R. *Physical Review B* **75**(7) February (2007).

[91] Drouhin, H.-J., Fishman, G., and Wegrowe, J.-E. *Physical Review B* **83**(11), 1–4 March (2011).

[92] Shi, J., Zhang, P., Xiao, D., and Niu, Q. *Physical Review Letters* **96**(7), 1–4 February (2006).

[93] Sugimoto, N., Onoda, S., Murakami, S., and Nagaosa, N. *Physical Review B* **73**(11), 1–4 March (2006).

[94] Zhang, P., Wang, Z., Shi, J., Xiao, D., and Niu, Q. *Physical Review B* **77**(7), 1–9 February (2008).

[95] Wong, A. and Mireles, F. *Physical Review B* **81**(8), 1–11 February (2010).

[96] BenDaniel, D. and Duke, C. *Physical Review* **152**(2), 683–692 December (1966).

[97] Harrison, W. *Physical Review* **123**(1), 85–89 July (1961).

[98] Bottegoni, F., Drouhin, H.-j., Fishman, G., and Wegrowe, J.-e. In *SPIE Proceedings vol. 8100*, volume 2, 810012–810012–4, (2011).

[99] Messiah, A. *Quantum Mechanics*. North Holland Publishing Company, Amsterdam, (1962).

[100] Dresselhaus, G. *Physical Review* **100**(2), 580–586 October (1955).

[101] Rougemaille, N., Drouhin, H.-J., Richard, S., Fishman, G., and Schmid, A. *Physical Review Letters* **95**(18), 1–4 October (2005).